ADAPTIVE BEAMFORMING DETECTION PERFORMANCE ON KOREAN SHORT PERIOD INTERFERING EVENTS

Wen-Wu Shen

Texas Instruments,
Incorporated

Prepared for:

Advanced Research Projects Agency
Air Force Technical Applications Center

7 May 1975

ALEX(01)-TR-75-02

ADAPTIVE BEAMFORMING DETECTION PERFORMANCE ON KOREAN SHORT-PERIOD INTERFERING EVENTS

TECHNICAL REPORT NO. 2

VELA NETWORK EVALUATION AND AUTOMATIC PROCESSING RESEARCH

Prepared by
Wen-Wu Shen

TEXAS INSTRUMENTS INCORPORATED
Equipment Group
Post Office Box 6015
Dallas, Texas 75222

Prepared for

AIR FORCE TECHNICAL APPLICATIONS CENTER
Alexandria, Virginia 22314

Sponsored by

ADVANCED RESEARCH PROJECTS AGENCY
Nulcear Monitoring Research Office
ARPA Program Code No. 5F10
ARPA Order No. 2551

7 May 1975

Acknowledgment: This research was supported by the Advanced Research Projects Agency, Nuclear Monitoring Research Office, under Project VELA-UNIFORM, and accomplished under the technical direction of the Air Force Technical Applications Center under Contract No. F08606-75-C-0029.

ALEX(01)-TR-75-02

ADAPTIVE BEAMFORMING DETECTION PERFORMANCE ON KOREAN SHORT-PERIOD INTERFERING EVENTS

TECHNICAL REPORT NO. 2

VELA NETWORK EVALUATION AND AUTOMATIC PROCESSING RESEARCH

Prepared by
Wen-Wu Shen

TEXAS INSTRUMENTS INCORPORATED
Equipment Group
Post Office Box 6015
Dallas, Texas 75222

Prepared for

AIR FORCE TECHNICAL APPLICATIONS CENTER
Alexandria, Virginia 22314

Sponsored by

ADVANCED RESEARCH PROJECTS AGENCY
Nulcear Monitoring Research Office
ARPA Program Code No. 5F10
ARPA Order No. 2551

7 May 1975

Acknowledgment: This research was supported by the Advanced Research Projects Agency, Nuclear Monitoring Research Office, under Project VELA-UNIFORM, and accomplished under the technical direction of the Air Force Technical Applications Center under Contract No. F08606-75-C-0029.

UNCLASSIFIED

SECURITY CLASSIFICATION OF THIS PAGE (When Data Entered)

REPORT DOCUMENTATION PAGE

READ INSTRUCTIONS BEFORE COMPLETING FORM

1 REPORT NUMBER	2 GOVT ACCESSION NO.
3 RECIPIENT'S CATALOG NUMBER	
4 TITLE (and Subtitle) ADAPTIVE BEAMFORMING DETECTION PERFORMANCE ON KOREAN SHORT PERIOD INTERFERING EVENTS	5 TYPE OF REPORT & PERIOD COVERED: Technical
	6 PERFORMING ORG. REPORT NUMBER: ALEX(01)-TR-75-02
7 AUTHOR(s): Wen-Wu Shen	8 CONTRACT OR GRANT NUMBER(s): F08606-75-C-0029
9 PERFORMING ORGANIZATION NAME AND ADDRESS: Texas Instruments Incorporated, Equipment Group, Dallas, Texas 75222	10 PROGRAM ELEMENT, PROJECT, TASK AREA & WORK UNIT NUMBERS: VELA T/5705/B/ETR
11 CONTROLLING OFFICE NAME AND ADDRESS: Advanced Research Projects Agency, Nuclear Monitoring Research Office, Arlington, Virginia 22209	12 REPORT DATE: 7 May 1975
	13 NUMBER OF PAGES: 68
14 MONITORING AGENCY NAME & ADDRESS (if different from Controlling Office): Air Force Technical Applications Center, VELA Seismological Center, Alexandria, Virginia 22314	15 SECURITY CLASS (of this report): UNCLASSIFIED
	15a DECLASSIFICATION/DOWNGRADING SCHEDULE

16 DISTRIBUTION STATEMENT (of this Report)

APPROVED FOR PUBLIC RELEASE, DISTRIBUTION UNLIMITED

17 DISTRIBUTION STATEMENT (of the abstract entered in Block 20, if different from Report)

18 SUPPLEMENTARY NOTES

ARPA Order No. 2551

19 KEY WORDS (Continue on reverse side if necessary and identify by block number)

Seismology
Korean Short-Period Array
Maximum likelihood
Adaptive multichannel filtering
Mixed-event separation

20 ABSTRACT (Continue on reverse side if necessary and identify by block number)

This report presents the results obtained from applying an adaptive time-domain maximum likelihood multichannel filtering processor to simulated mixed-event data from the Korean short-period array. Comparisons between adaptive processing and beamsteering are based on the amplitude rise of the beam output after the arrival of an on-azimuth signal buried in a stronger off-azimuth interfering event. Four mixed-event simulations

DD FORM 1 JAN 73 1473 EDITION OF 1 NOV 65 IS OBSOLETE

UNCLASSIFIED

SECURITY CLASSIFICATION OF THIS PAGE (When Data Entered)

20. Continued
with various adaptive-filter operational specifications are preformed in this report.

ABSTRACT

This report presents the results obtained from applying an adaptive time-domain maximum likelihood multichannel filtering processor to simulated mixed-event data from the Korean short-period array. Comparisons between adaptive processing and beamsteering are based on the amplitude rise of the beam output after the arrival of an on-azimuth signal buried in a stronger off-azimuth interfering event. Four mixed-event simulations with various adaptive-filter operational specifications are performed in this report.

ACKNOWLEDGMENTS

I wish to thank Mr. Thomas E. Barnard, who directed this work, Mr. Terence W. Harley, who provided encouragement and technical discussions which improved the quality of the report, and Mrs. B. C. Taylor, who typed the manuscript.

TABLE OF CONTENTS

LIST OF FIGURES

LIST OF FIGURES
(Continued)

LIST OF TABLES

SECTION I
INTRODUCTION

A. PURPOSE OF THIS STUDY

The first objective of the signal estimation task in the VELA Network Evaluation and Automatic Processing Research program (Project VT/5705) is to investigate and report on new techniques for optimally detecting the arrival of a second seismic event buried in the coda of a first-arriving event at various signal-to-noise ratios.

This report deals with results obtained from operating a maximum likelihood adaptive beamforming system on Korean short-period data for mixed-event separation.

B. DESCRIPTION OF KOREAN SHORT-PERIOD ARRAY

Figure I-1 depicts the geometrical configuration of the Korean Short-Period Array, which is a 19-element hexagonal array. Table I-1 gives the array sensor locations.

C. DESCRIPTION OF THE MAXIMUM LIKELIHOOD ADAPTIVE FILTER ALGORITHM

The adaptive filter output $y(t)$ at time t is formed by applying a convolution filter to each channel and summing the outputs of all filters:

$$y(t) = \sum_{i=1}^{M} \sum_{j=-N}^{N} a_i(j)\, x_i(t-j) \qquad (I-1)$$

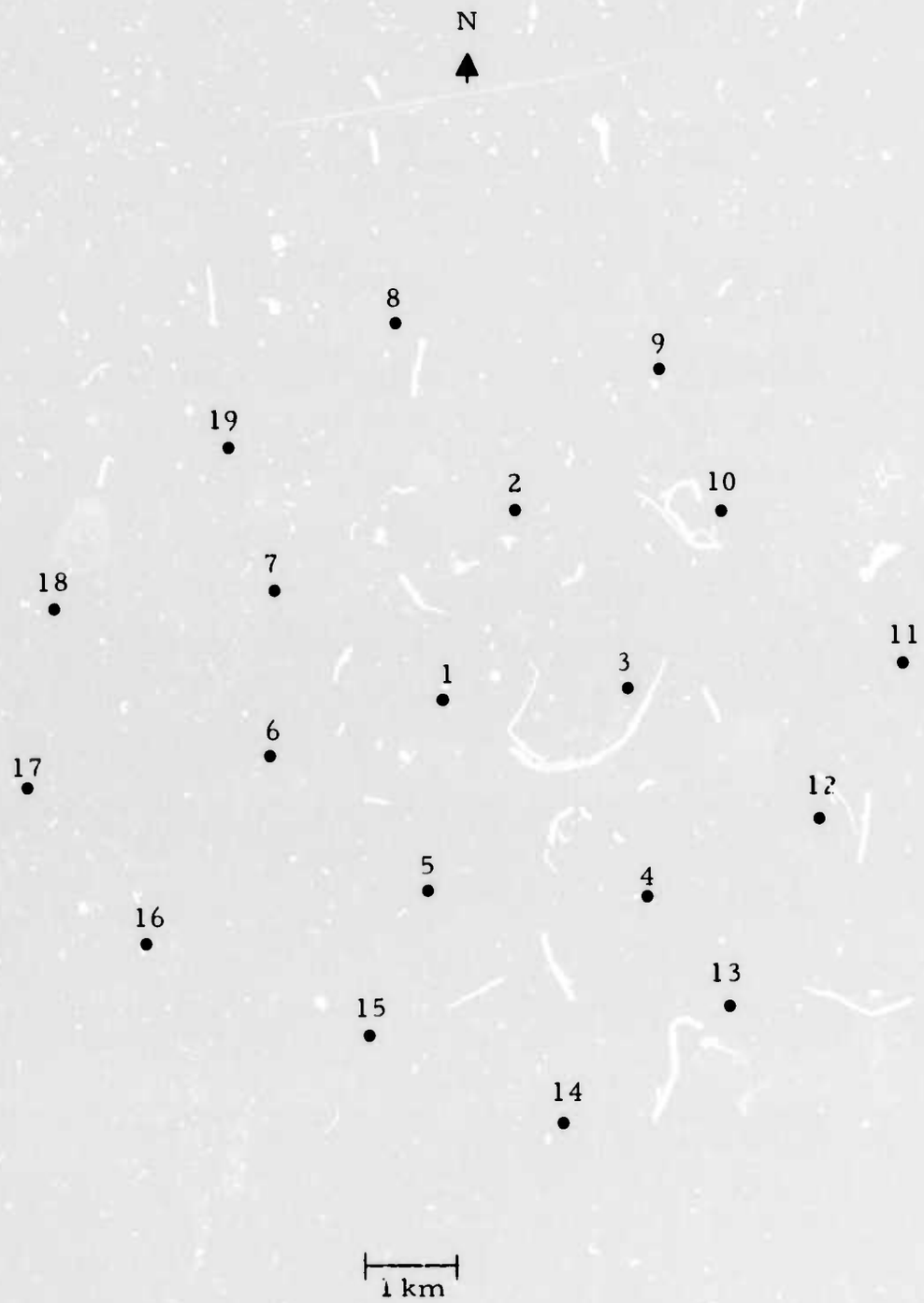

FIGURE I-1

KOREAN SHORT-PERIOD ARRAY GEOMETRY

TABLE I-1

KOREAN SHORT-PERIOD SENSOR LOCATIONS
(Reference Location (37° 27' 14" N, 127° 55' 24" E))

Sensor Number	East (X) Kilometers	North (Y) Kilometers
1	-2.34	2.24
2	-1.55	4.35
3	-0.26	2.37
4	-0.05	-0.01
5	-2.53	0.11
6	-4.32	1.61
7	-4.24	3.48
8	-2.85	6.52
9	0.13	6.00
10	0.86	4.34
11	2.90	2.60
12	1.93	0.85
13	0.81	-1.25
14	-1.08	-2.57
15	-3.25	-1.57
16	-5.80	-0.47
17	-7.10	1.29
18	-6.75	3.33
19	-4.72	5.11

where $a_i(j)$ is the filter weight for the i-th channel at a lag of j sample points, $x_i(t-j)$ is the value of the channel i at time t-j, M is the number of channels, and $2N+1$ is the total length of the filter in points. Prior to forming the filter output, each channel is time-shifted to time-align energy arriving from the desired steer direction.

The adaptive filter weights are updated by the following algorithm:

$$a_i^{new}(j) = a_i^{old}(j) + \frac{2\mu\, y(t)\, [\bar{x}(t-j) - x_i(t-j)]}{\sum_{i=1}^{M} \sum_{j=-N}^{N} x_i^2(t-j)} \qquad \text{(I-2)}$$

where

$$\bar{x}(t-j) = \frac{1}{M} \sum_{i=1}^{M} x_i(t-j) \qquad \text{(I-3)}$$

and μ controls the adaptation rate. This update algorithm incorporates the maximum likelihood constraints.

In vector form, the adaptive-beamforming filter update equation may be written

$$A(t+\Delta t) - A(t) = \frac{2\mu\, X^T A(\bar{X}-X)}{X^T X} \quad , \qquad \text{(I-4)}$$

where the superscript T denotes vector transpose, and where the filter weight vector A, the data vector X, and the beamsteer output vector $\bar{X}$ are, respectively,

$$A = \begin{bmatrix} \begin{bmatrix} a_1(-N) \\ \vdots \\ a_M(-N) \end{bmatrix} \\ \vdots \\ \begin{bmatrix} a_1(0) \\ \vdots \\ a_M(0) \end{bmatrix} \\ \vdots \\ \begin{bmatrix} a_1(N) \\ \vdots \\ a_M(N) \end{bmatrix} \end{bmatrix}, \quad X = \begin{bmatrix} \begin{bmatrix} x_1(t+N) \\ \vdots \\ x_M(t+N) \end{bmatrix} \\ \vdots \\ \begin{bmatrix} x_1(t) \\ \vdots \\ x_M(t) \end{bmatrix} \\ \vdots \\ \begin{bmatrix} x_1(t-N) \\ \vdots \\ x_M(t-N) \end{bmatrix} \end{bmatrix}, \quad \text{and } \overline{X} = \begin{bmatrix} \begin{bmatrix} \overline{x}(t+N) \\ \vdots \\ \overline{x}(t+N) \end{bmatrix} \\ \vdots \\ \begin{bmatrix} \overline{x}(t) \\ \vdots \\ \overline{x}(t) \end{bmatrix} \\ \vdots \\ \begin{bmatrix} \overline{x}(t-N) \\ \vdots \\ \overline{x}(t-N) \end{bmatrix} \end{bmatrix}. \tag{I-5}$$

The objective of maximum likelihood adaptive beamforming is to reduce the average squared filter output

$$\overline{y^2(t)} = \overline{(A^T X)\ (X^T A)} = A^T \overline{XX^T} A \tag{I-6}$$

subject to a set of signal-preservation constraints on the filter vector A. After preshifting the input channels to time-align energy from the look direction, these constraints can be written

$$\sum_{i=1}^{M} a_i(j) = d(j) \qquad (j = -N, \ldots, -1, 0, 1, \ldots N), \tag{I-7}$$

where the constraints d(j) specify a convolution filter having the desired frequency response on a signal from the steer direction. For the adaptive beamforming employed in this study, a flat frequency response is specified by setting

$$d(j) = \delta_{jo} \qquad (j = -N, \ldots, -1, 0, 1, \ldots N), \qquad \text{(I-8)}$$

where δ_{ij} is the Kronecker delta operator

$$\delta_{ij} = \begin{cases} 1 & \text{if } i = j \\ 0 & \text{if } i \neq j \ . \end{cases} \qquad \text{(I-9)}$$

D. ORGANIZATION OF REPORT

Section II presents the results of mixed-event simulations which examine the possibility that adaptive beamforming can detect signals buried in off-azimuth interfering events when the conventional beamsteer processor cannot. The simulation process is performed by scaling two individually recorded data samples and summing them to create a composite sample used in the adaptive-filter update procedure. The adaptive filter is then applied to the two data samples separately to form two separate beam outputs which are subsequently added to create a composite beam output. The detection capability of adaptive processing is determined from a measurement of the amplitude rise on the composite trace after the on-azimuth event arrival. In this report, the results from four mixed-event simulations with various adaptive-filter operational specifications using Korean short-period data are presented. Long-period results using ALPA data have been included in a previous report (Barnard and O'Brien, 1974).

Section III presents the conclusions of this study. References are given in Section IV.

SECTION II
INTERFERING-EVENT RESULTS

A. DISCUSSION

The ability of adaptive beamforming to detect an on-azimuth event buried in stronger off-azimuth interfering events has been successfully demonstrated using Alaskan Long-Period Array data (Barnard and O'Brien, 1974). In this long-period study, maximum likelihood time-domain adaptive beamforming in one simulation achieved a 6 dB amplitude rise after the arrival of an on-azimuth signal in the presence of an interfering event 30 dB above the target signal at the single-sensor level. For Rayleigh waves, on the average, adaptive beamforming provided an array gain of 12 dB (0.6 magnitude units) over beamsteering. In addition to the detection improvement for the on-azimuth signal buried in the off-azimuth interfering events, adaptive beamforming also provided a reasonably accurate estimate of the on-azimuth signal's maximum peak-to-peak amplitude in the long-period results, where the error in estimating the on-azimuth signal strength was less than 0.1 magnitude units. These promising results suggest the use of this particular algorithm for P-wave interfering-event separation.

The next subsection describes the mixed-event simulation procedure. Subsection C discusses the results obtained from the Korean short-period array data. These results are limited to the four mixed-event simulations conducted during this contract period with various adaptive-filter operational specifications. A brief summary of the results is presented in Subsection D.

B. SIMULATION PROCEDURE

In the situations where two wavetrains from two separate events pass an array simultaneously, these wavetrains will overlap to form mixed events. Array processing techniques attempt to separate the mixed events by steering the array toward the target signal to attenuate the off-azimuth interfering-event energy. However, as the data are actually recorded, there is no evaluation method which can reliably isolate the energy contribution from each of the two mixed events. Hence, the most realistic method to evaluate array-processing techniques such as beamsteering or adaptive beamforming is to rely on a simulation procedure in which two data samples, each containing one signal, are added to create a composite sample including the overlapped wavetrains of the on-azimuth signal and the off-azimuth interfering event. Such a simulation can be designed to include a number of parameters through which various physical situations can be studied. In specifying the parameters for a mixed-event simulation, the relative signal strength of the two events, the incoming directions of the two signals, and the time separation of their arrivals can be controlled to illustrate the real-world situations.

Figure II-1 presents a schematic diagram for the simulation procedure. As shown in the figure, the basic mixed-event simulation procedure sums two data samples: one contains the on-azimuth signal and the other includes the off-azimuth interfering event. Before summing the two samples to form a composite sample, each input channel of the two samples passes through the same zero-phase prefilter. The on-azimuth signal sample is time-shifted to time-align the target event. The interfering event, on the other hand, can be shifted from its true azimuth and apparent P-wave velocity to the desired incoming azimuth and velocity before beamforming so that the interfering event will appear to come from a fictitious location in the simulation.

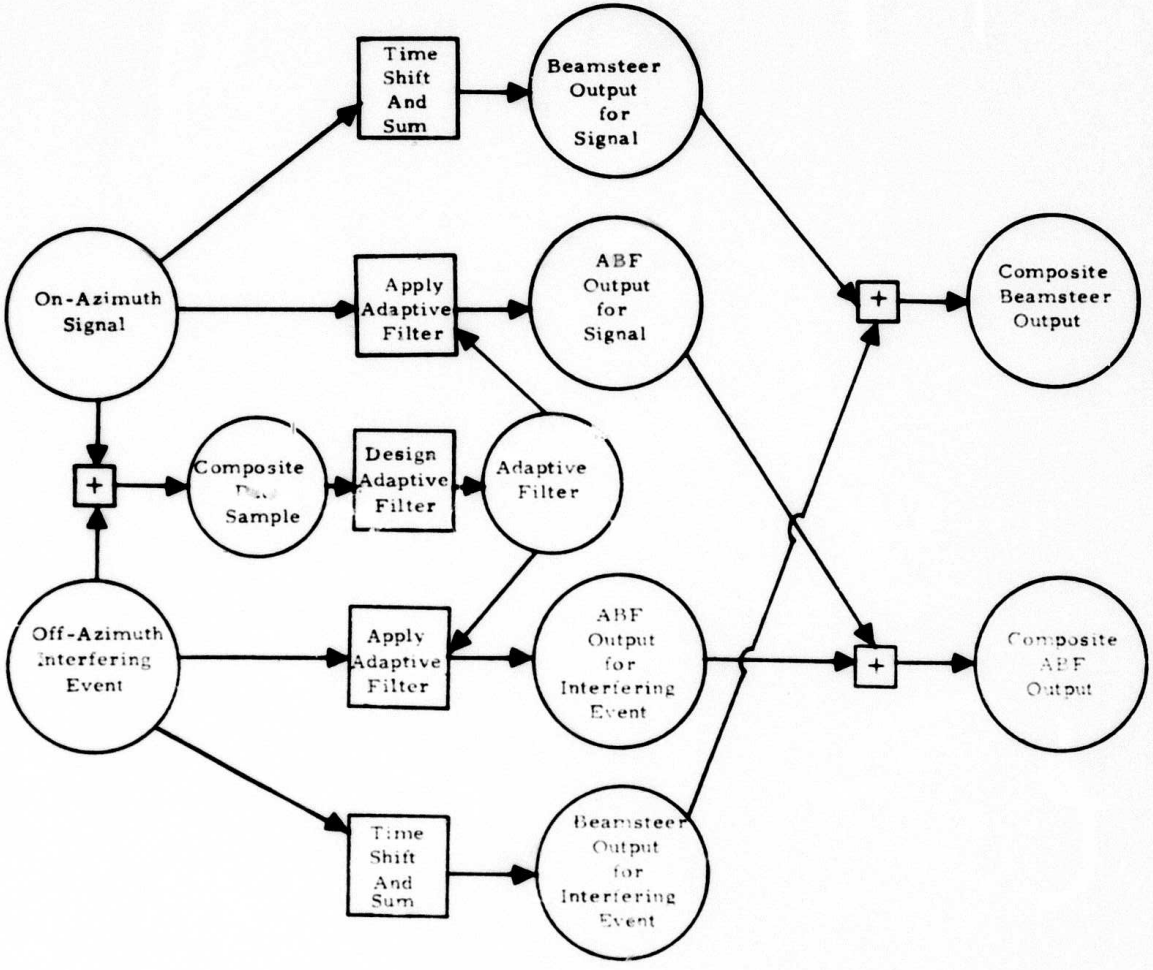

FIGURE II-1

BLOCK DIAGRAM OF INTERFERING-EVENT SIMULATION PROCEDURE

The shifting of the interfering event azimuth and velocity is accomplished by re-adjusting the time delays for the input channels of the interfering-event sample. Following the formation of the composite sample, a time-domain adaptive multi-channel filter is designed from it. Initially, a beamsteer filter is used, and, after initialization, the adaptive filter updates its filter weights according to the update equation

$$A(t+\Delta t) = A + \frac{2\mu X^T A\,(\bar{X}-X)}{X^T X} \quad .$$

The computer software package can simultaneously update the filter sets for as many as twenty adaptive convergence rates μ in a single processing run. The adaptive filter sets are subsequently applied to each individual data sample to form separate beam outputs for the on-azimuth signal and the off-azimuth interfering event. Finally, the ABF beam for the on-azimuth signal and the ABF beam for the off-azimuth interfering event are combined to form the composite ABF trace. The time-shift-and-sum beams for the on-azimuth signal and the off-azimuth interfering event are formed similarly and subsequently are added to form the beamsteer composite trace. The composite traces in the simulation are the only beam outputs which are available in real-world situations. The evaluation of adaptive processing performance relative to beamsteering is based on a comparison of the composite traces for the time-shift-and-sum and adaptive beam outputs. However, in order to facilitate an understanding of the beamforming processes involved in the mixed-event situations, the individual sample beams for the on-azimuth signal and the interfering event are plotted along with the composite trace for the beamsteer output and the specified adaptive-beam outputs. Evaluation of adaptive beamforming performance relative to beamsteering is accomplished on the basis of the composite-trace beams.

C. RESULTS

1. General

The principal goal of this subsection is to examine the detection performance of adaptive beamforming relative to beamsteering for short-period interfering events simulated by adding two suitably preprocessed data samples from the Korean Short-Period Array. A secondary objective is to evaluate the reliability of the peak-to-peak amplitude on the composite-sample adaptive filter output as an estimate of the on-azimuth signal's peak-to-peak amplitude. Because this is the first application of adaptive multichannel filtering to Korean Short-Period Array data, this evaluation also provides an opportunity to gain an understanding of the optimal choice of processing parameters such as the prefilter applied to the data before beamforming and the azimuthal separation between the interfering event and the target event. In most cases, the adaptive-filter length is 31 points per channel. A shorter filter length has merit in on-line system operation if it does not substantially degrade ABF performance. Therefore, other shorter adaptive filter lengths such as a 15-point filter length and a 7-point filter length are also tested. At various points in this subsection, four events are used to simulate mixed events. Table II-1 lists the pertinent data for these events. Each of these events is considerably stronger than the background noise level. Signal similarity varies from event to event and from passband to passband. It will be discussed as the need arises. The convergence rate μ for the adaptive filter update is allowed to vary in each processing simulation in order to observe the effect of the convergence rate on adaptive processing detection gain relative to beamsteering.

2. Prefilters Used

Since both the signal and noise spectra for the Korean Short-Period Array data are still not well understood at this time, a number of

TABLE II-1

EVENTS USED IN INTERFERING-EVENT SIMULATION
(FROM 1973 PDE BULLETIN)

Origin Time Day/Hr. Min. Sec.	Location		m_b	Region	Azimuth (Deg.)	Epicentral Delta (Deg.)	Apparent P-Wave Velocity at Array (km/sec)
	Lat. (Deg.)	Long. (Deg.)					
119/00. 59. 33. 8	6. 3S	129. 9E	5. 3	Banda Sea	177. 16	43. 79	13. 86
125/01. 35. 19. 0	8. 2S	156. 4E	5. 4	Solomon Islands	143. 69	52. 85	15. 43
145/13. 17. 26. 0	53. 2N	161. 3W	4. 9	South of Alaska	47. 64	49. 45	15. 10
169/17. 45. 43. 7	42. 5N	146. 0E	5. 8	Off Coast of Hokkaido	64. 30	14. 71	9. 08

prefilters have been designed for the mixed-event simulations. Figures II-2 through II-6 show prefilter responses in dB for the five prefilters employed in this study. Figure II-2 displays the response for the prefilter with a 1.0-2.0 Hz passband centered at 1.5 Hz. The response at 0.0 Hz is below -120 dB so that the d.c. bias can be removed. Figure II-3 shows the response of a prefilter with the lower-frequency passband 0.5 - 1.5 Hz centered at 1.0 Hz. The corresponding response for a prefilter with a wider passband (1.0-3.0 Hz) is illustrated in Figure II-4. Figures II-5 and II-6 display the response of two prefilters with 0.5-1.0 Hz and 1.25-1.75 Hz passbands, respectively.

3. First Mixed-Event Simulation

To simulate the first mixed event, the data samples for the Banda Sea event and for the event from off the coast of Hokkaido are summed. The formerevent is from day 119 and serves as the on-azimuth signal, while the latter event is from day 169 and serves as the off-azimuth interfering event. Start times for the two data samples were chosen so that the day 119 on-azimuth event arrives about 30 seconds later than the day 169 interfering event. The interfering-event azimuth was shifted from 64.30° to 357.16° to achieve a 180° azimuthal separation from the target event, which has a 177.16° arrival azimuth relative to the Korean Array. The P-wave velocity for the day 169 interfering event was also shifted from the 9.08 km/sec true apparent velocity to the 13.86 km/sec target event velocity. Twelve sites (all but sites 1, 2, 5, 9, 10, 11 and 15) constitute the channel inputs to the beamformers. The event separation level is adjusted by scaling either the on-azimuth signal or the off-azimuth interfering event.

In this first mixed-event simulation, the data traces from the day 119 event were scaled so that the averaged peak-to-peak amplitude of the target signal at the single-sensor level is 12 dB less than the corresponding averaged amplitude of the day 169 interfering event.

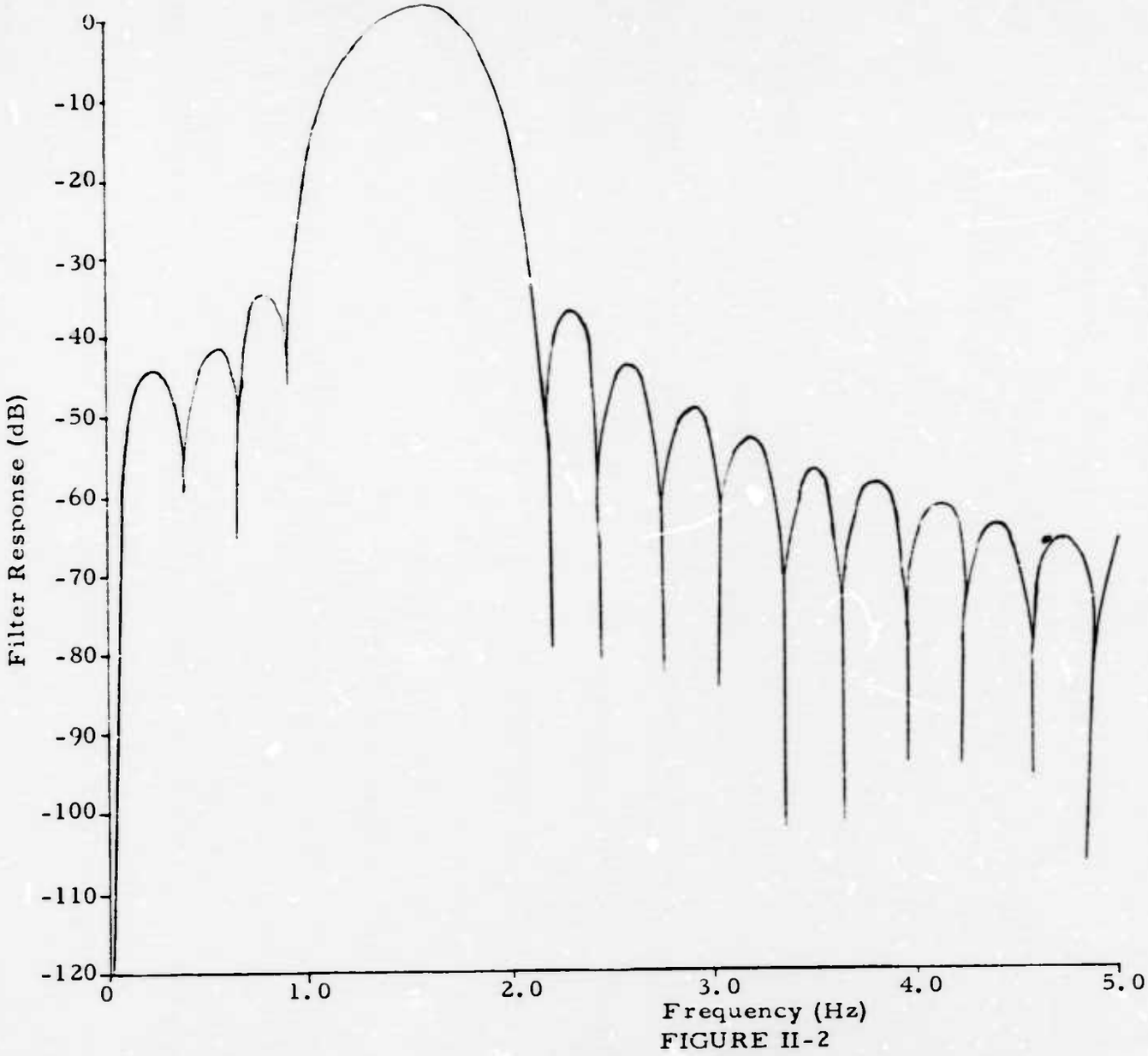

FIGURE II-2

SHORT-PERIOD PREFILTER RESPONSE (dB)
(1.0-2.0 Hz PASSBAND)

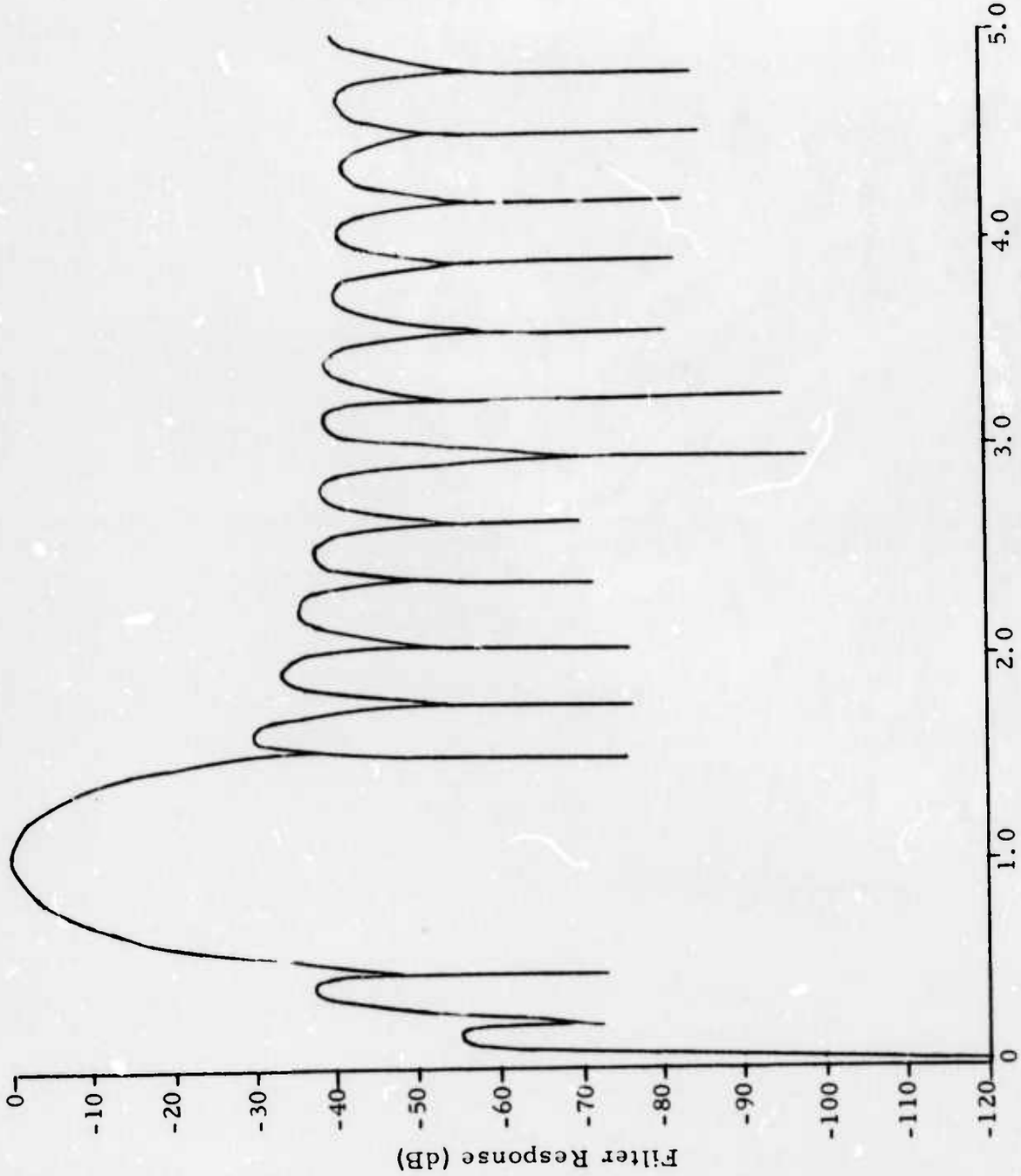

FIGURE II-3

SHORT-PERIOD PREFILTER RESPONSE (dB)
(0.5-1.5 Hz PASSBAND)

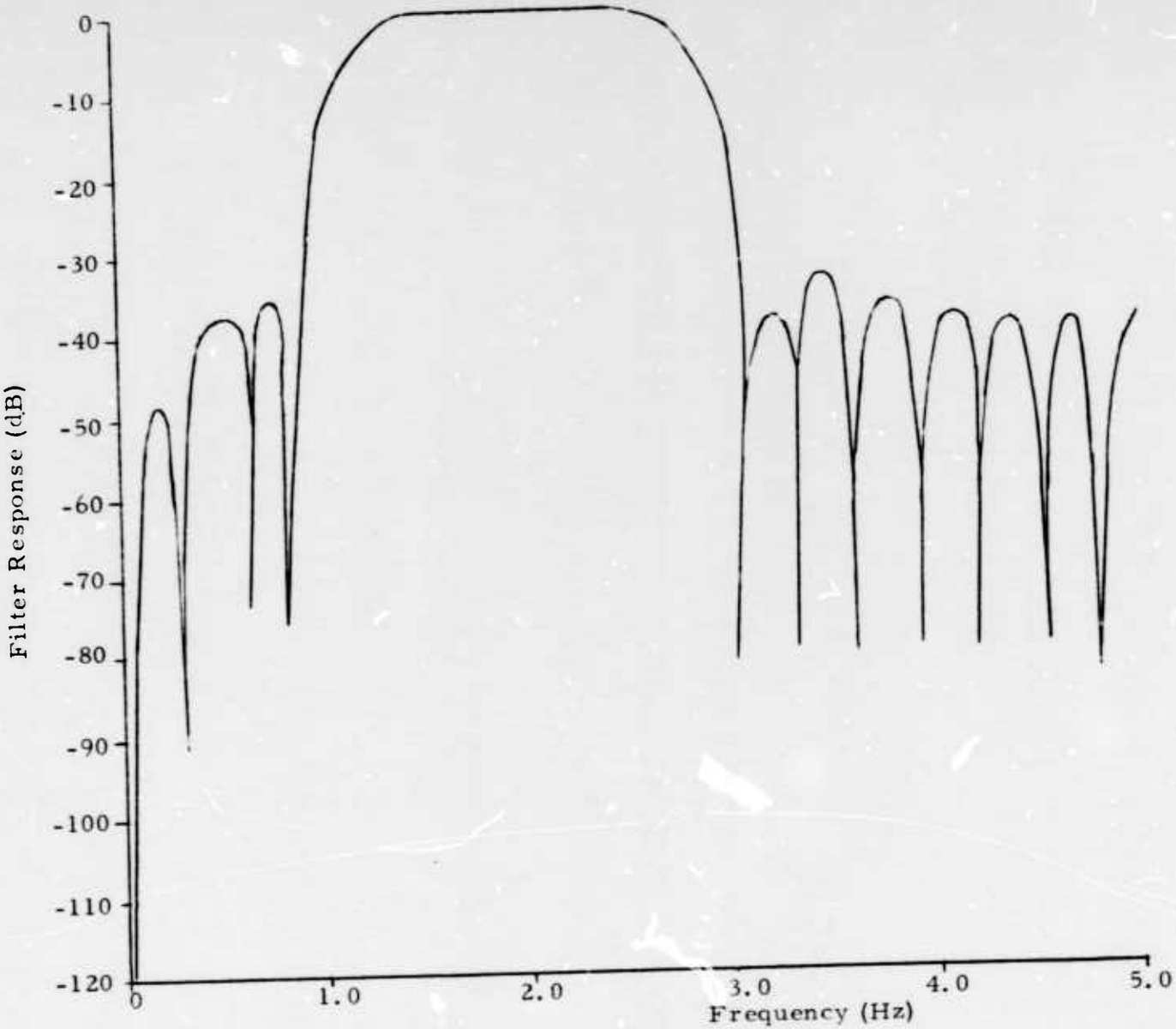

FIGURE II-4

SHORT-PERIOD PREFILTER RESPONSE (dB)
(1.0-3.0 Hz PASSBAND)

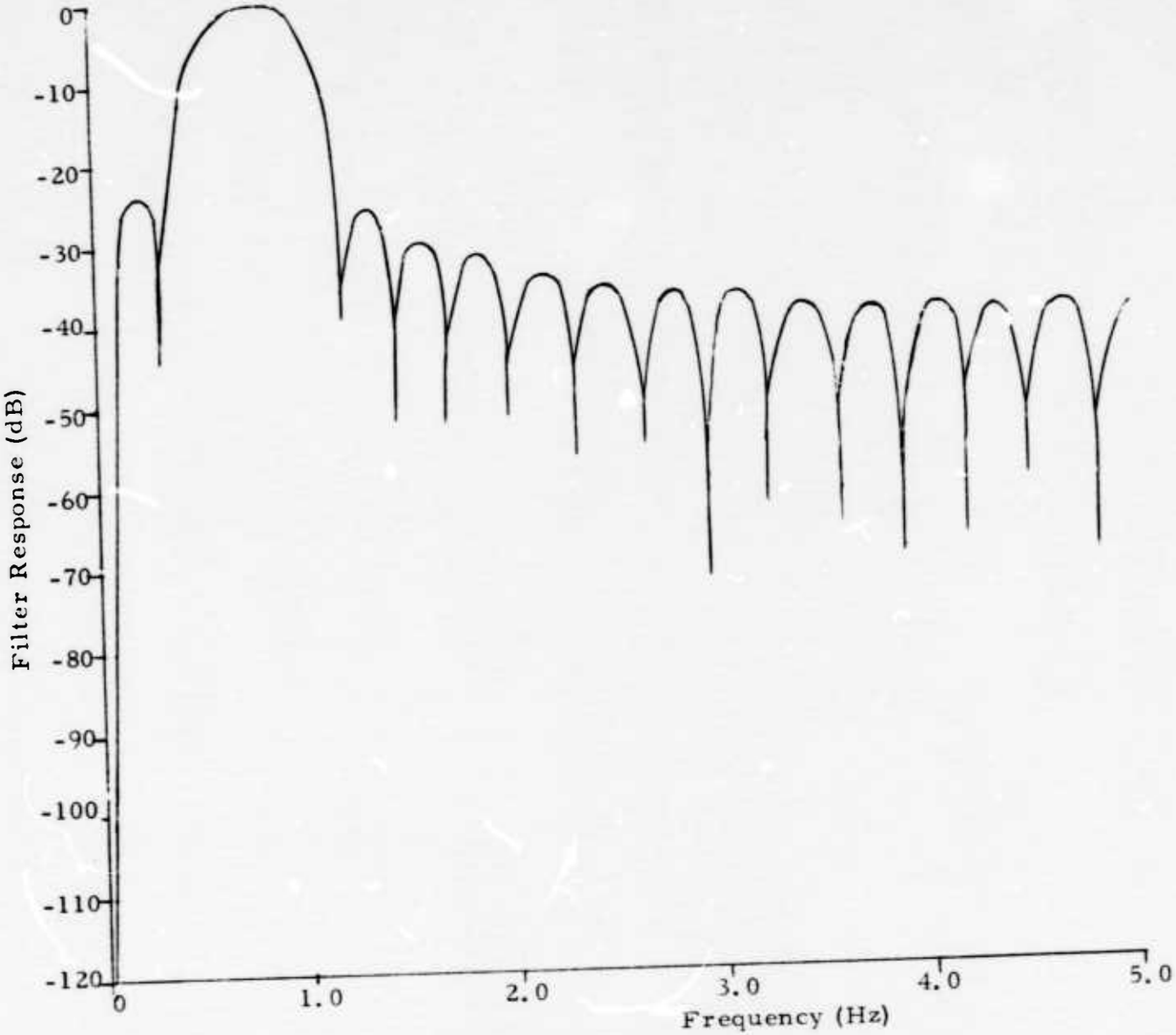

FIGURE II-5

SHORT-PERIOD PREFILTER RESPONSE (dB)
(0.5-1.0 Hz PASSBAND)

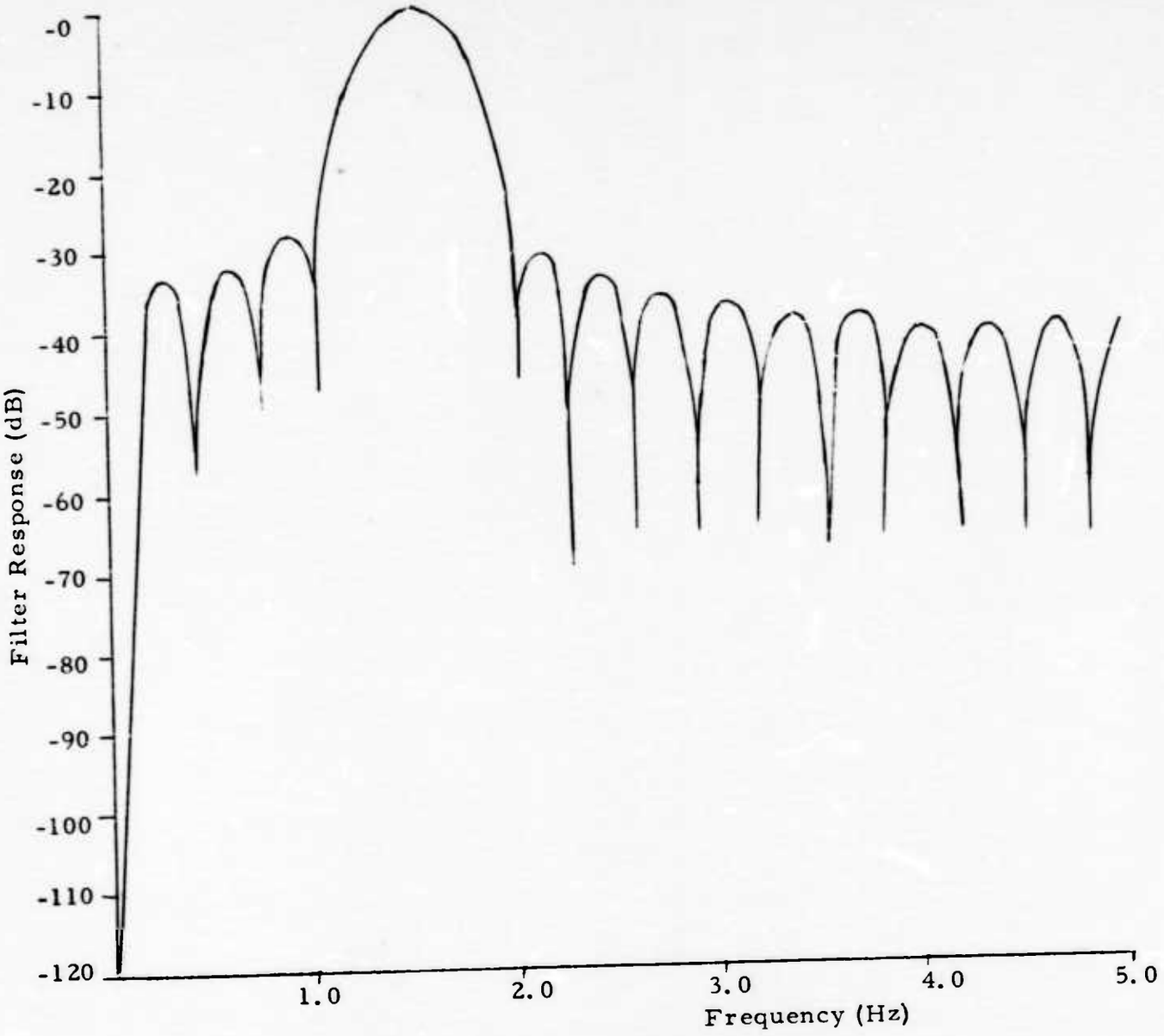

FIGURE II-6

SHORT-PERIOD PREFILTER RESPONSE (dB)
(1.25-1.75 Hz PASSBAND)

Figure II-7 illustrates the beamsteer output traces for the first mixed-event simulation. The upper trace is the beamsteer output for the day 119 data sample with the on-azimuth signal. The middle trace is the beamsteer output for the day 169 data sample with the interfering event shifted to a 357.16° azimuth. The bottom trace is the composite-sample beamsteer output formed by summing the upper and middle traces. The input traces for the day 119 event were scaled to a level 12 dB below that of the day 169 interfering event so that the composite trace for the adaptive beamformer has a 6 dB amplitude rise. Figure II-8 shows the adaptive beam outputs for the convergence rate $\mu = 0.3$. Signal similarity for the day 169 interfering event is poor and the relative channel strength varies with time. This event lasts considerably longer than a typical P-wave event. The amplitude rise on the ABF composite trace is 6 dB, while the beamsteer output yielded 3.8 dB for the corresponding peak-to-peak measurement. In this case, the best ABF improvement is 2.2 dB over beamsteering on the basis of peak-to-peak amplitude measurements on the composite traces.

In Figure II-8, the composite trace has a 6 dB borderline detection. Once the detection is declared, the next most important consideration in evaluating the adaptive beamforming performance is the accuracy with which the peak-to-peak amplitude on the composite trace reflects the peak-to-peak amplitude of the on-azimuth signal. Measurement of the peak-to-peak amplitudes on the upper trace and composite trace for the on-azimuth signal window yields the same amplitude, as shown in Figure II-8. Therefore, the amplitude on the composite-trace adaptive beam for this mixed event furnishes an accurate bodywave magnitude estimate for the detected on-azimuth signal if the adaptive resulting apparent period of signal remains unchanged.

As mentioned earlier, adaptive beamforming yields only 2.2 dB improvement over beamsteering on the basis of peak-to-peak amplitude measurements on the composite traces in Figures II-7 and II-8. However, it does not

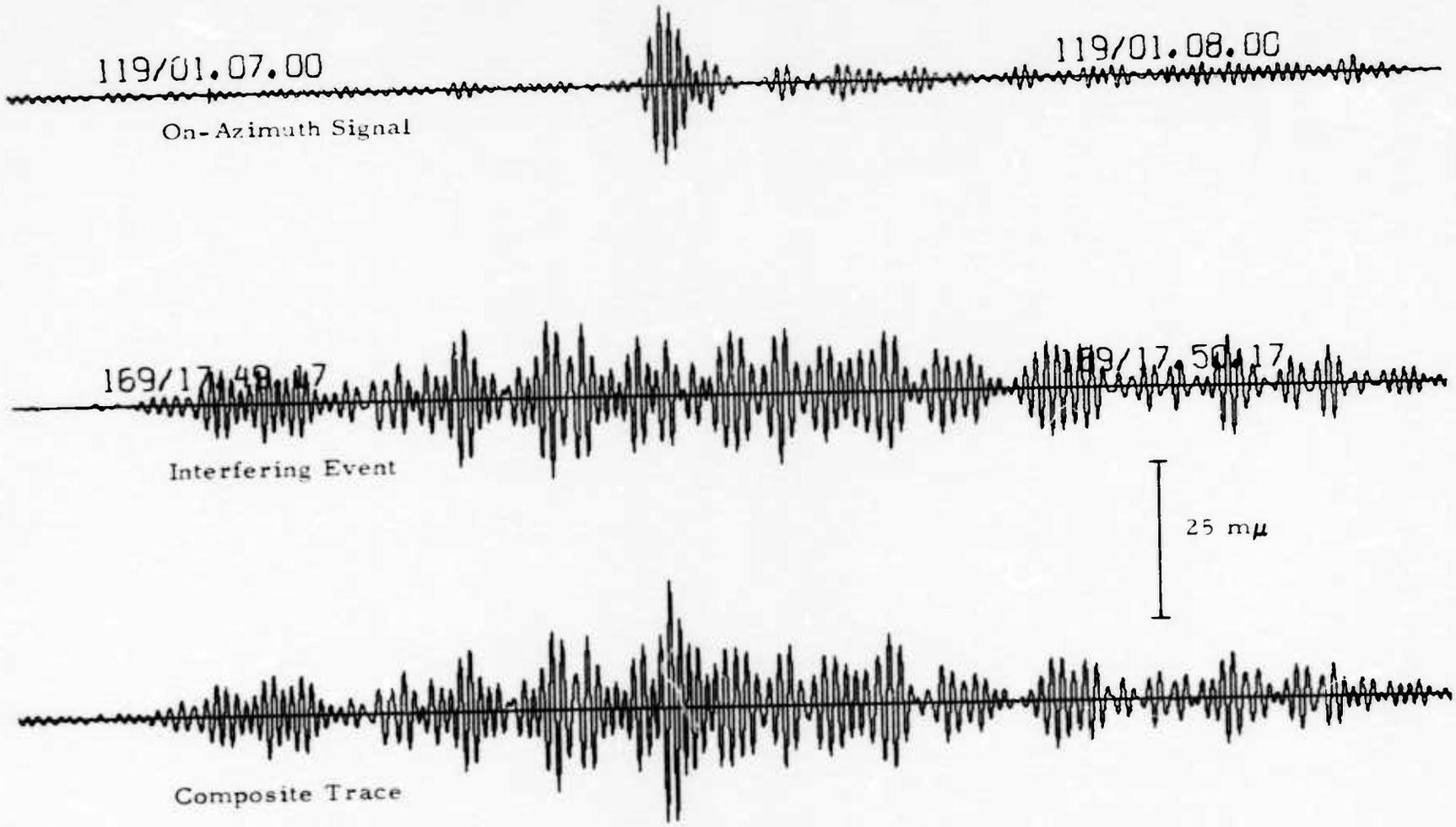

FIGURE II-7

BEAMSTEER OUTPUT FOR THE MIXED EVENT FROM DAYS 119 AND 169 OF 1973
(Signal Azimuth 177.16°, Interfering Event Azimuth 357.16°, Signal Apparent Velocity 13.86 km/sec, Interfering Event 12 dB above the On-Azimuth Signal, 1.0-2.0 Hz Passband)

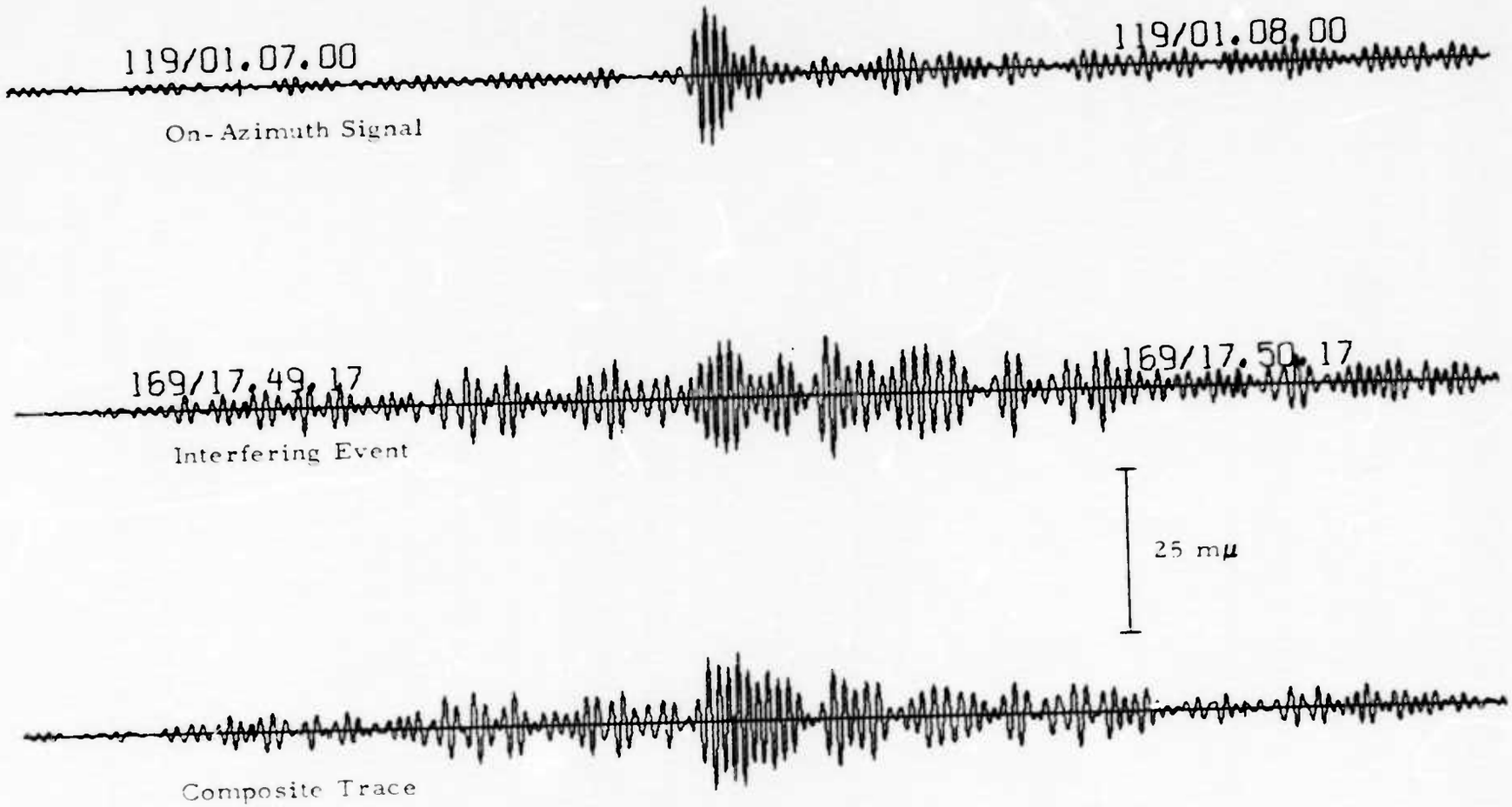

FIGURE II-8

ABF OUTPUT FOR THE MIXED EVENT FROM DAYS 119 AND 169 OF 1973 (μ = 0.3, Signal Azimuth 177.16°, Interfering Event Azimuth 357.16°, Signal Apparent Velocity 13.86 km/sec, Interfering Event 12 dB Above the On-Azimuth Signal, 1.0-2.0 Hz Passband)

necessarily follow that the beamsteer output will be able to produce a 6 dB amplitude rise for an on-azimuth event with a bodywave magnitude 0.11 units higher. To demonstrate this fact, the day 169 on-azimuth event was re-scaled so that the beamsteer output on the composite trace is able to achieve the same 6 dB amplitude rise on the basis of peak-to-peak amplitude measurements over the same time windows. For this reason, Figure II-9 displays the beamsteer output traces. The composite trace in this figure has the same 6 dB amplitude rise as the corresponding adaptive trace in Figure II-8. But the off-azimuth event input channels in Figure II-9 are only 7.6 dB above the on-azimuth event at the single sensor level. Hence, comparing the single sensor levels for Figure II-8 and those for Figure II-9, adaptive beamforming actually yields 4.4 dB improvement over beamsteering in this mixed-event simulation. Figure II-10 shows the corresponding adaptive beam output at the 7.6 dB event-separation level, where the amplitude rise on the composite trace is 8.5 dB.

At the 7.6 dB event separation level used to produce the results of Figures II-9 and II-10, the composite-trace adaptive filter output again gives a more accurate estimate of the event strength. For the beamsteer output on the composite trace in Figure II-9, the peak-to-peak amplitude over the on-azimuth signal window is 2.2 dB, or 0.11 magnitude units, higher than that of the upper trace due to the energy from the interfering event. In the case of the adaptive filter output, the peak-to-peak amplitude on the composite trace in Figure II-10 is about 1.1 dB lower than the corresponding amplitude on the upper trace.

To examine adaptive beamforming performance at various convergence rates for this mixed-event simulation, Table II-2 tabulates the amplitude-rise results and the ratios of the composite-trace amplitude to the corresponding upper-trace amplitude over the on-azimuth signal window for the various beams. The results in this table are from the output beams at the

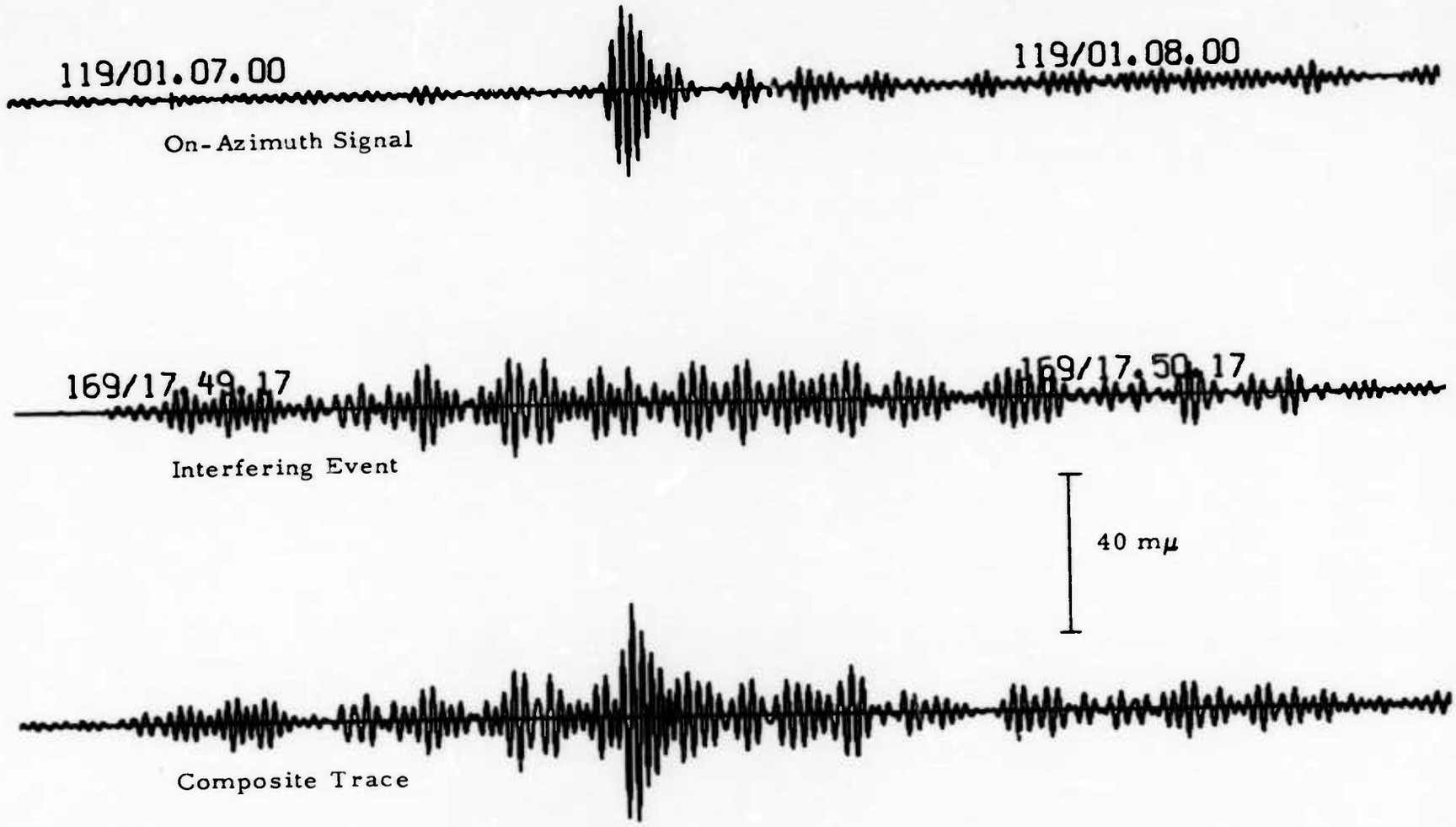

FIGURE II-9

BEAMSTEER OUTPUT FOR THE MIXED EVENT FROM DAYS 119 AND 169 OF 1973
(Signal Azimuth 177.16°, Interfering Event Azimuth 357.16°, Signal Apparent Velocity 13.86 km/sec, Interfering Event 7.6 dB Above the On-Azimuth Signal, 1.0-2.0 Hz Passband)

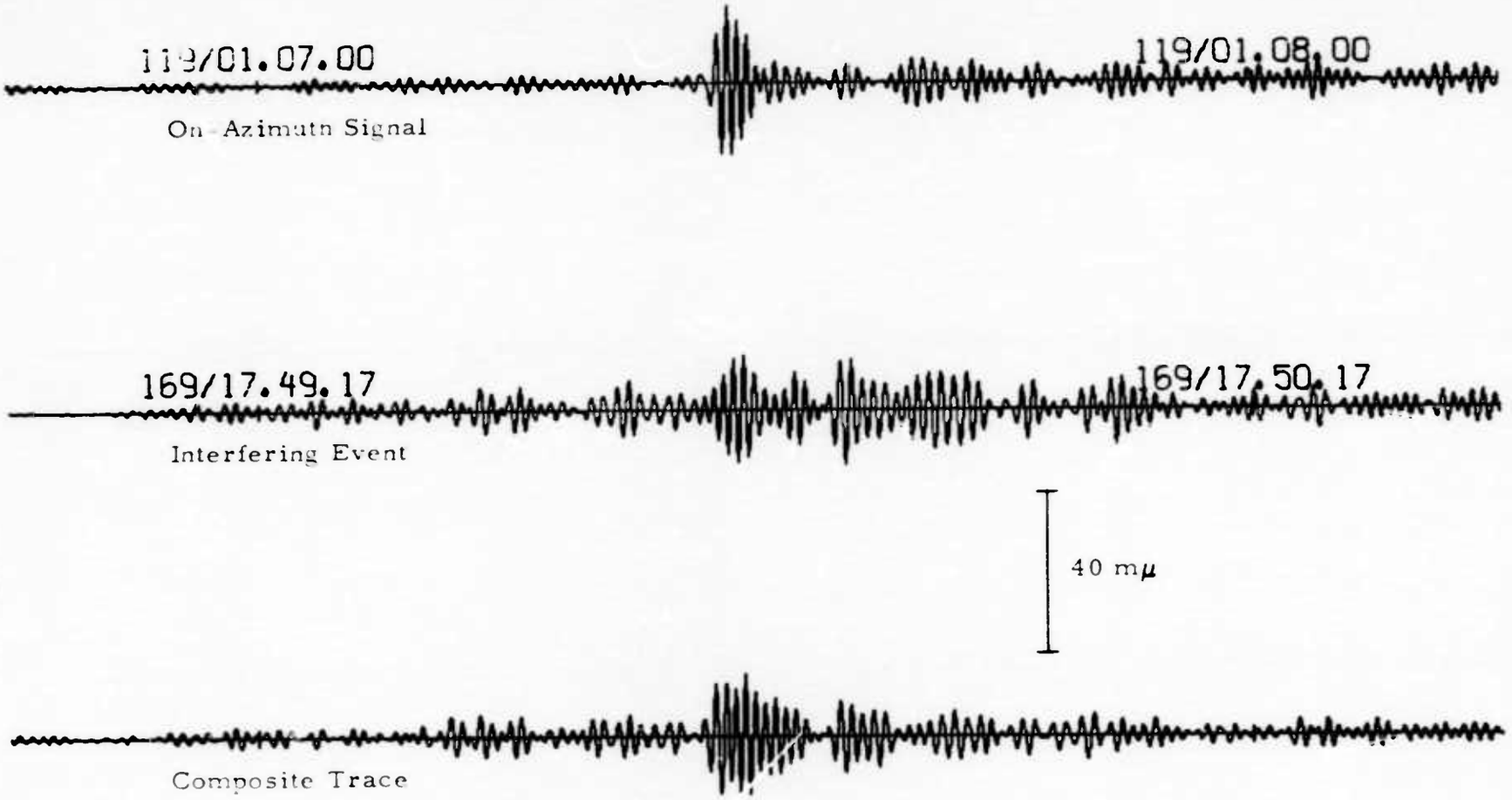

FIGURE II-10

ABF OUTPUT FOR THE MIXED EVENT FROM DAYS 119 AND 169 OF 1973 (μ = 0.3, Signal Azimuth 177.16°, Interfering Event Azimuth 357.16°, Signal Apparent Velocity 13.86 km/sec, Interfering Event 7.6 dB Above the On-Azimuth Signal, 1.0-2.0 Hz Passband)

TABLE II-2

PEAK-TO-PEAK AMPLITUDE RATIOS (dB)
ON THE COMPOSITE TRACES FOR BEAMSTEERING
AND VARIOUS ADAPTIVE CONVERGENCE RATES
FROM DAY 119 AND 169 OF 1973 (Signal Azimuth 177.16°, Interfering
Event Azimuth 357.16°, Signal Apparent Velocity 13.86 km/sec,
Event 12 dB Above the On-Azimuth Signal, 1.0-2.0 Hz Passband)

	Beamsteering	Adaptive Convergence Rates							
		0.005	0.01	0.05	0.1	0.2	0.3	0.4	0.5
Amplitude Rise (dB)	3.8	3.3	3.2	3.8	4.6	5.2	6	4.6	3.9
Ratio of Composite-Trace Amplitude to Upper-Trace Amplitude for On-Azimuth Signal (dB)	3.4	3.6	3.5	2.6	1.3	0.6	0	-1.3	-2.0

12 dB event separation level. Some of these results have been discussed previously in comparing the detection thresholds for beamsteering and adaptive beamforming. At low convergence rates, adaptive beamforming suppresses the on-azimuth signal more than the off-azimuth interfering event. Therefore, the amplitude rise values for the adaptive convergence rates less than 0.1 are slightly lower than those of the beamsteer output, and the beamsteer amplitude rise is equal to that of adaptive beamforming at the convergence rate $\mu = 0.05$. For the convergence rates greater than 0.1, adaptive beamforming is able to suppress the interfering event more than the on-azimuth signal. This fact results in the ABF improvements over beamsteering. The maximum amplitude rise in the table is 6 dB at the convergence rate $\mu = 0.3$. For the convergence rates greater than 0.3, the interfering event amplitude remains about the same, but the on-azimuth signal amplitude is lower than that of the adaptive beam for $\mu = 0.3$. As a result, the amplitude rise is lower. The ratio of the composite trace signal amplitude to the upper-trace amplitude for the time-shift-and-sum beams is 3.4 dB. For adaptive beamforming, this ratio is greater than 3.4 dB for the convergence rates less than or equal to 0.01 and is equal to zero for the adaptive beams at $\mu = 0.3$, where the amplitude rise is the highest. At the adaptive convergence rates greater than 0.3, the composite-trace signal is attenuated.

Various ABF operational specifications were tested for this mixed-event simulation using the events from days 119 and 169. These specifications include the prefilter passbands and the number of adaptive filter weights per channel. Table II-3 tabulates the amplitude rise on the composite-trace for the beamsteer and adaptive beam outputs. The on-azimuth signal attenuation as well as the interfering event suppression by adaptive beamforming relative to those of beamsteering were also included in the next-to-the-last two columns of the table.

TABLE II-3

AMPLITUDE RISE VALUES FOR VARIOUS CASES OF THE FIRST MIXED EVENT SIMULATION (ON-AZIMUTH EVENT FROM DAY 119, INTERFERING EVENT FROM DAY 169)

Pre-filter Pass band (Hz)	ABF Filter Weights Per Channel (Points)	Azimuthal Separation	Best ABF Convergence Rate(μ)	Event Separation(dB)	Beam-steer Amplitude Rise(dB)	Best ABF Amplitude Rise(dB)	ABF On-Azimuth Signal Attenuation Relative to Beam-steering(dB)	ABF Off-Azimuth Interfering Event Suppression Relative to Beam-steering(dB)	ABF Detection Gain(dB)
0.50-1.50	31	180°	0.01	-12.0	1.6	1.4	0.9	0.7	-0.2
1.00-2.00	31	180°	0.30	-7.6	6.0	8.5	5.3	7.8	2.5
1.00-2.00	31	180°	0.30	-12.0	3.8	6.0	5.0	7.2	2.2
1.00-2.00	31	180°	0.30	-18.0	0.8	2.9	4.3	6.4	2.1
1.00-3.00	31	180°	0.30	-12.0	3.4	5.4	3.1	5.1	2.0
1.25-1.75	31	180°	0.30	-12.0	4.0	6.0	5.0	7.0	2.0
1.25-1.75	7	180°	0.40	-18.0	0.3	1.8	5.5	7.0	1.5
1.25-1.75	31	180°	0.05	-18.0	0.6	1.5	1.2	2.1	0.9

In the 0.5-1.5 Hz passband, the waveform similarity for the on-azimuth event of day 119 is poor and the relative strength of the channels varies with time. Therefore, both the beamsteer and adaptive amplitude rise values are the poorest among the passbands shown in the table. The ABF improvement relative to beamsteering is also the poorest for this mixed-event study. Two things occurred with this passband. One is that adaptive beamforming was not able to suppress the interfering event at any of the convergence rates specified. The other is that, at the higher convergence rates, mutual cancellation is responsible for the negative results relative to beamsteering at the higher convergence rates.

In one case, a 7-point adaptive filter length was used for the 1.25-1.75 Hz passband. At the one-decisecond sampling interval, the 7-point filter length covers one cycle at the center frequency for that passband. In comparison with the results in the next row of the table, the 0.6 dB increase in the ABF gain is probably not enough to justify using that adaptive filter length. However, the best convergence rate for this filter length is $\mu = 0.4$ in contrast to $\mu = 0.05$ for the 31-point filter length, which had mutual cancellation at the higher convergence rates. If operating at the high convergence rates only, this is worth noting.

In concluding this first mixed-event simulation, the adaptive amplitude-rise results are, in general, about 2.0 dB better than for beamsteering. The waveform similarity and the time stability of the relative channel strength are also poor for the day 169 interfering event. The fact that the envelope shape for the input channels varies significantly across the array makes it difficult for the ABF processor to suppress the interfering event. In terms of the ABF detection improvement relative to beamsteering, adaptive beamforming can reduce the bodywave detection threshold by about 0.2 magnitude units from the beamsteer level for this mixed-event simulation.

4. Second Mixed-Event Simulation

The second mixed-event simulation employs the same Banda Sea event used in the first mixed-event study as the on-azimuth signal and uses the Alaskan event from day 145 as the off-azimuth interfering event. Originally, the interfering event has a 47.64° azimuth and a 15.1 km/sec P-wave velocity. In this simulation, the true azimuth of this event was shifted to 357.16° and 87.16°, while its true velocity was shifted to that of the on-azimuth signal. The start times for both samples were adjusted so that the on-azimuth signal arrives about 18 seconds later than the interfering event. This interfering event lasts about 30 seconds, considerably less than the first one from day 169. Fourteen sites were used for the input channels (all but sites 9, 10, 11, 18, and 19).

Initially, the interfering-event azimuth was shifted to 357.16° and the on-azimuth signal was scaled so that the interfering event is about 18 dB above the target signal at the single-sensor level. No 6 dB amplitude rise was achieved on either the beamsteer as the ABF output. Subsequently, the single-sensor input level for the on-azimuth signal was raised to 12 dB less than that of the interfering event. Using a filter length of 31 points per channel at this event-separation level, adaptive beamforming was still unable to achieve a 6 dB amplitude rise. However, using a 7-point-long adaptive filter and shifting the interfering event azimuth to 87.16° or 90° separation between the two events, adaptive beamforming is able to suppress the interfering event enough to achieve a 6 dB amplitude rise at the event-separation level where the interfering event is 16 dB above the on-azimuth signal at the single-sensor level. Figure II-11 displays the beamsteer output, where the amplitude rise is -1.6 dB on the composite trace. The corresponding adaptive beams for $\mu = 0.5$ are shown in Figure II-12. A 6 dB amplitude rise is achieved on the composite-trace beam. At this high convergence rate, adaptive beamforming suppresses the interfering event 11.5 dB more than beamsteering, but degrades the on-azimuth signal 3.8 dB relative to beamsteering. This fact results in the 7.7 dB detection gain for this simulation. The signal amplitude on the ABF

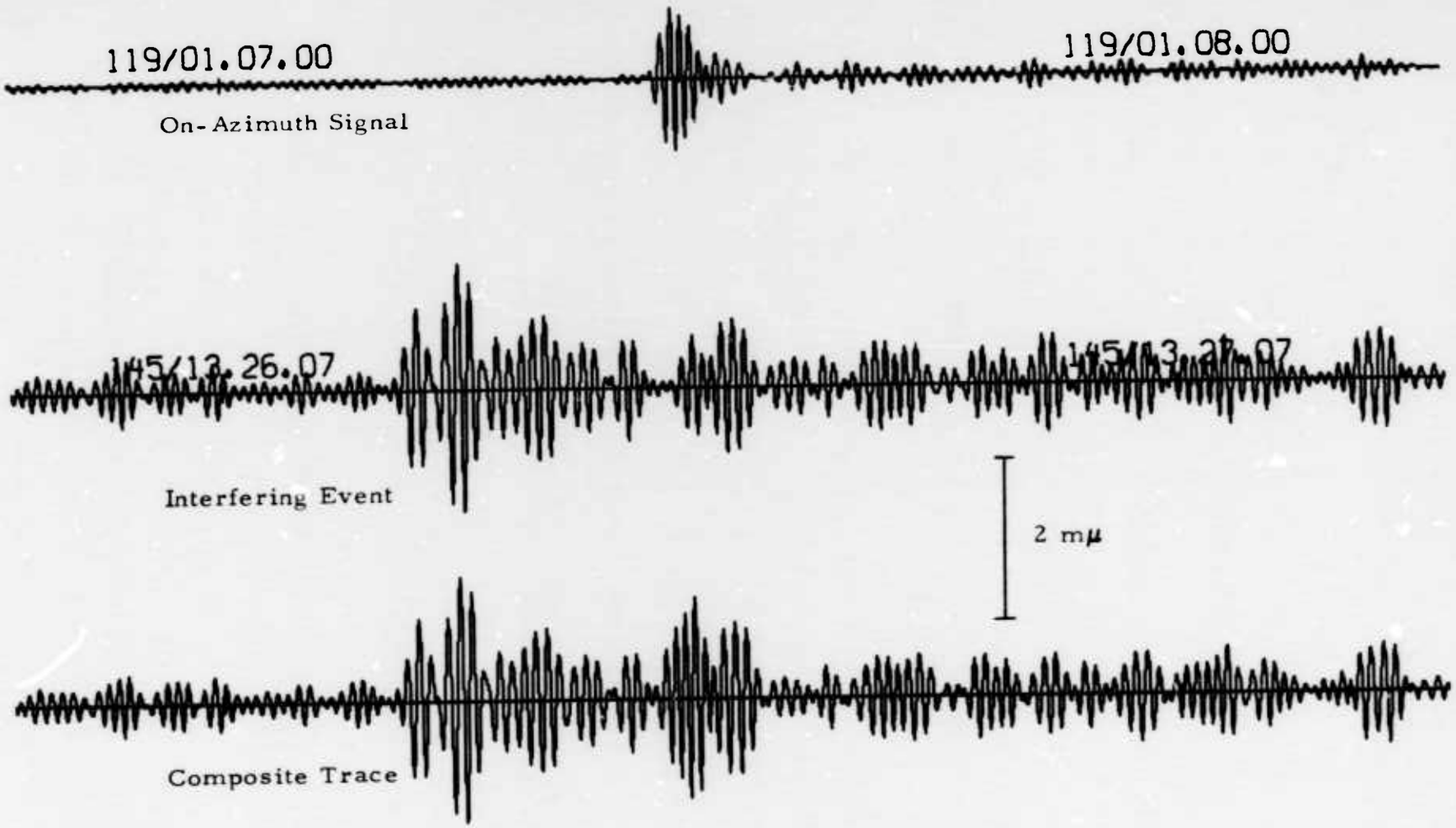

FIGURE II-11

BEAMSTEER OUTPUT FOR THE MIXED EVENT FROM DAYS 119 AND 145 OF 1973
(Signal Azimuth 177.16°, Interfering Event Azimuth 87.16°, Signal Apparent Velocity 13.86 km/sec, Interfering Event 16 dB Above the On-Azimuth Signal, 1.0-2.0 Hz Passband)

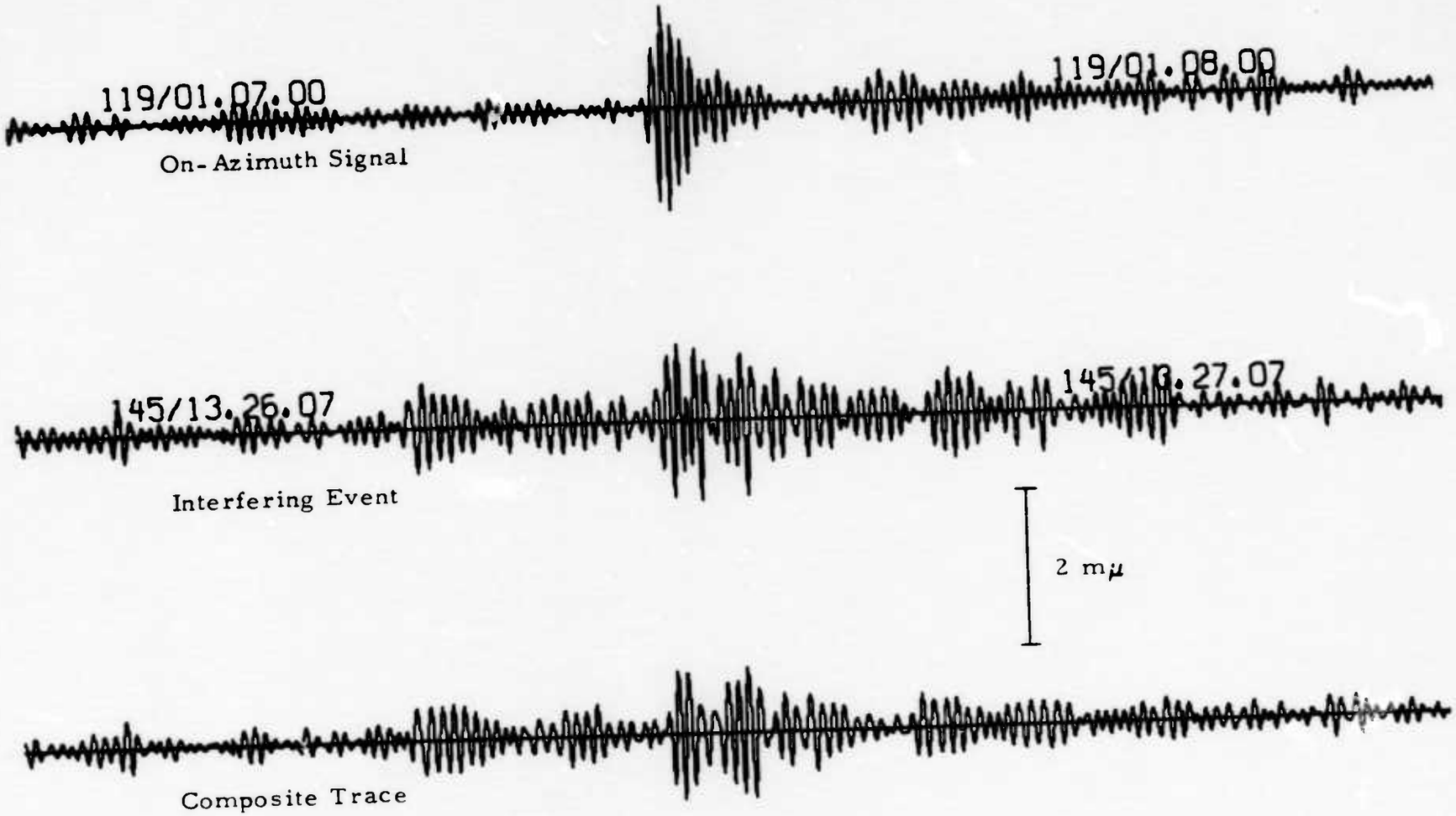

FIGURE II-12

ABF OUTPUT FOR THE MIXED EVENT FROM DAYS 119 AND 145 OF 1973
(μ = 0.5, Signal Azimuth 177.16°, Interfering Event Azimuth 87.16°, Signal Apparent Velocity 13.86 km/sec, Interfering Event 16 dB Above the On-Azimuth Signal, 7-Point Adaptive Filter Length, and 1.0-2.0 Hz Passband)

composite trace is 3.5 dB lower than the upper-trace amplitude. This reduction is due to relatively severe mutual cancellation of the two interfering events. As a matter of fact, the beamsteer output on the composite trace for the on-azimuth signal was 2.9 dB higher than on the upper trace because of the interfering-event energy. Consequently, the actual composite-trace signal degradation by the ABF processor relative to beamsteering is about 1 dB. In order to find the detection threshold reduction for this case, the event-separation level was re-adjusted so as to achieve a 6 dB amplitude rise on the beamsteer output. Figure II-13 shows the time-shift-and-sum beams when the interfering event is 5 dB above the on-azimuth signal at the single-sensor level. In other words, the threshold for a 6 dB amplitude rise is 11 dB, or .55 magnitude units lower for adaptive beamforming than for beamsteering. Figure II-14 shows the corresponding adaptive beams, where an 18.8 dB amplitude rise is achieved in the composite trace.

Table II-4 tabulates the amplitude-rise results for various ABF operational specifications in this mixed-event simulation. Using the 1.0-2.0 Hz passband, the 31-point adaptive filter length at 180° azimuthal separation yielded a 2.1 dB improvement relative to beamsteering. A slightly lower improvement value is obtained using a 7-point filter length. Greater improvement values are obtained at a 90° azimuthal separation for both the 31-point and 7-point filter lengths. Using the narrower 1.25-1.75 Hz passband, the detection gain is comparable with that of the 1.0-2.0 Hz passband at the 12 dB event separation level, but is 1.4 dB less for the larger 18 dB event separation level, as indicated in the table. A 6 dB ABF detection gain is achieved for the 1.0-3.0 Hz passband. This increased ABF improvement can be attributed to mutual cancellation on the time-shift-and-sum beam. This case is an exception. For the 0.5-1.5 Hz passband, the results are, in general, the worst among the passbands shown. A partial explanation for these results is the poor waveform similarity and the time-varying relative channel strengths for the on-azimuth signal in this passband (as discussed in the last mixed-event simulation.) A 15-point adaptive filter length was also specified in order to compare its adaptive filter performance with that of the 31-point filter length. In this case, a 3.5 dB lower

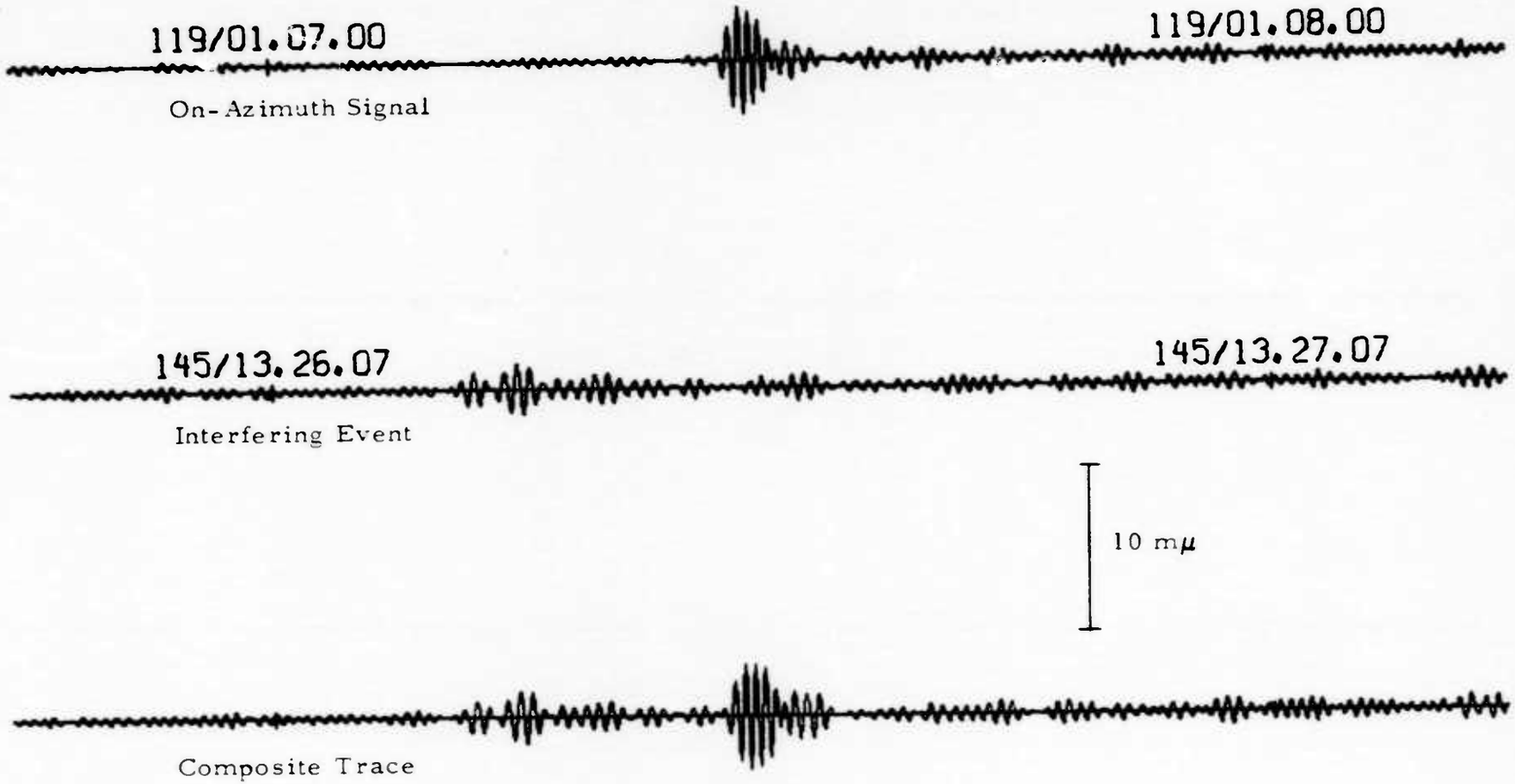

FIGURE II-13

BEAMSTEER OUTPUT FOR THE MIXED EVENT FROM DAYS 119 AND 145 OF 1973
(Signal Azimuth 177.16°, Interfering Event Azimuth 87.16°, Signal Apparent Velocity 13.86 km/sec, Interfering Event 5 dB Above the On-Azimuth Signal, 1.0-2.0 Hz Passband)

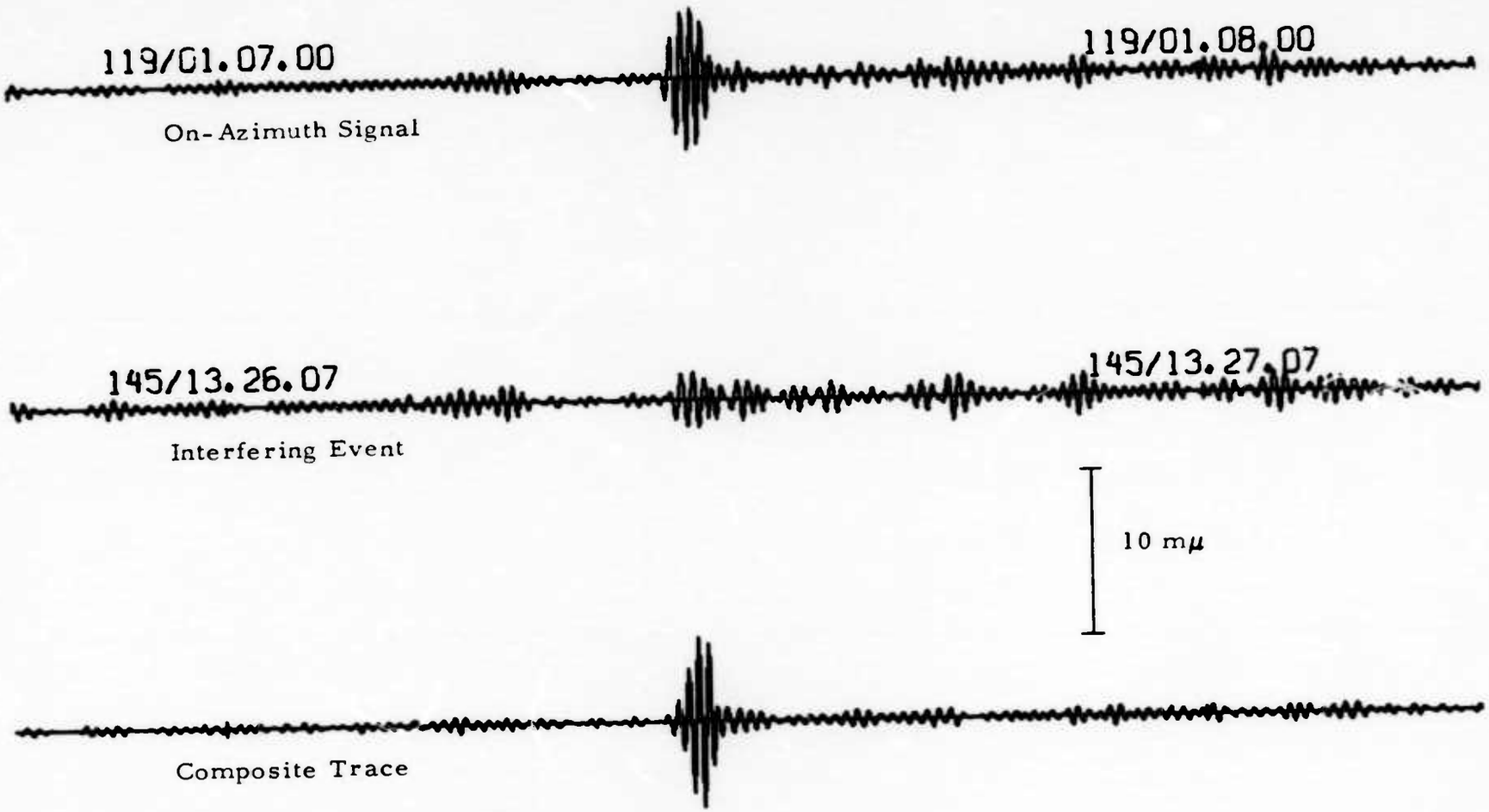

FIGURE II-14

ABF OUTPUT FOR THE MIXED EVENT FROM DAYS 119 AND 145 OF 1973 (μ = 0.5, Signal Azimuth 177.16°, Interfering Event Azimuth 87.16°, Signal Apparent Velocity 13.86 km/sec, Interfering Event 5 dB Above the On-Azimuth Signal, 7-Point Adaptive Length, and 1.0-2.0 Hz Passband)

TABLE II-4

AMPLITUDE RISE VALUES FOR VARIOUS CASES OF THE MIXED-EVENT SIMULATION (ON-AZIMUTH EVENT FROM DAY 119, INTERFERING EVENT FROM DAY 145, 14 SITES)

Pre-filter Pass-band (Hz)	ABF Filter Weights Per Channel (Points)	Azi-muthal Separa-tion	Best ABF Conver-gence Rate(μ)	Event Separa-tion(dB)	Beam-steer Ampli-tude Rise(dB)	Best ABF Ampli-tude Rise(dB)	ABF On-Azimuth Signal Attenutation Relative to Beam-steering(dB)	ABF Off-Azimuth Interfering Event Suppression Relative to Beam-steering(dB)	ABF Detec-tion Gain(dB)
1.00-2.00	7	90°	0.50	-12.0	0.3	8.0	3.9	11.6	7.7
1.00-2.00	7	90°	0.50	-16.0	-1.7	6.0	3.8	11.5	7.7
1.00-2.00	7	90°	0.50	-5.0	6.0	18.8	8.8	4.0	12.8
1.00-2.00	7	180°	0.10	-12.0	-0.9	0.3	2.7	3.8	1.1
1.00-2.00	31	90°	0.50	-12.0	0.3	4.5	4.7	8.9	4.2
1.00-2.00	31	180°	0.05	-12.0	-0.9	1.2	2.1	4.2	2.1
1.00-2.00	31	180°	0.50	-18.3	-3.9	0.0	8.5	12.4	3.9
1.25-1.75	31	180°	0.05	-12.0	1.1	3.5	2.0	4.4	2.4
1.25-1.75	31	180°	0.40	-18.3	-4.1	-1.5	7.3	9.8	2.5
1.00-3.00	31	180°	0.40	-18.3	-6.0	0.0	4.4	10.5	6.0
0.50-1.50	31	180°	0.40	-18.0	-3.8	-4.4	9.5	8.9	-0.6
0.50-1.50	15	180°	0.40	-18.9	-3.8	-7.9	7.0	2.9	-4.1

detection gain relative to the 31-point-filter length was obtained. The 180° azimuthal separation for this mixed-event from days 119 and 145 yielded only slightly better detection gains than the previous simulation using the events from days 119 and 169, even though the day 145 interfering event has better waveform similarity and less instability in relative channel strength. However, at a 90° azimuthal separation between the interfering event and the on-azimuth signal, an adaptive-beamforming amplitude rise 11 dB (0.55 magnitude units) higher than that of beamsteering was achieved with the same two events using a 7-point adaptive filter length. Comparison with the 0.1 m_b unit reduction achieved with a 180° azimuthal separation and a 31-point filter length suggests that adaptive beamforming performance varies considerably and depends strongly on the specific operational situation encountered.

5. Third Mixed-Event Simulation

The third mixed-event simulation combines the day 145 Alaskan event, which was used in the second mixed event simulation as an off-azimuth interfering event, and the day 125 event from the Solomon Islands region. The Alaskan event in this simulation serves as the on-azimuth signal, while the Soloman Islands event, with a 143.69° azimuth and a 52.85° epicentral delta relative to the Korean Short-Period Array, serves as the off-azimuth interfering event. The interfering event azimuth was shifted to 227.64° and, in some cases to 137.64° to achieve 180° and 90° azimuthal separation between the two events, while its apparent P-wave velocity was shifted to 15.10 km/sec, which is the on-azimuth event P-wave velocity. The start times for the two events were adjusted so that the on-azimuth signal arrives 20 seconds later than the interfering event. Two array configurations were employed: the 7-element inner-ring array and the 19-element field array.

Using the 7-site inner ring array (sites 1 through 7) and with the interfering-event azimuth shifted to 227.64°, the on-azimuth signal was initially scaled so that the interfering event is 18.8 dB above the on-azimuth signal at the single-sensor level. Neither the beamsteer nor the adaptive

processor achieved a 6 dB amplitude-rise value. In order to compare the detection thresholds between the ABF and beamsteer processors, as was done previously in the last two mixed-event simulations, the on-azimuth signal was scaled to 3.1 dB less than the interfering event at the single-sensor level so that a 6 dB amplitude-rise value for the ABF beam could be achieved. Figure II-15 displays the beamsteer output, where a 0.9 dB amplitude rise occurred on the composite-trace time-shift and-sum beam. The corresponding adaptive beams for the convergence rate $\mu = 0.5$ are shown in Figure II-16, where a 6dB amplitude rise occurred on the composite-trace output. Among the time-shift-and-sum beams in Figure II-15, the composite-trace on-azimuth signal is 3.9 dB less than on the upper trace, while in Figure II-16 the composite-trace on-azimuth signal amplitude is 0.2 dB less than that on the upper trace. Therefore, the ABF processing gain is mostly due to interfering event suppression. In order to achieve a 6 dB amplitude rise for beamsteering, the on-azimuth signal has to be re-scaled so that it is 2.4 dB above the interfering event at the single-sensor level. Figure II-17 shows the beamsteer output for this case. Because the input channels for the on-azimuth signal are higher than those of the interfering event, the composite-trace on-azimuth signal is essentially equal to that on the upper trace. Figure II-18 displays the corresponding adaptive beams, where the amplitude rise on the composite trace is 17.4 dB. In comparison with the beamsteer detection threshold, adaptive beamforming is able to reduce the detection level by 5.5 dB, equivalent to 0.28 magnitude units for this mixed event with the inner-ring array.

A number of cases were processed for this mixed-event simulation. Table II-5 tabulates the amplitude-rise results using the 7-site inner-ring array. In two cases, the interfering-event azimuth was shifted from 143.69° to 137.64° to achieve a 90° azimuthal separation between the two events. In two cases, an 11-point filter length was compared with a 31-point filter length. None of these provided a higher ABF gain than a 31-point filter with a 180° azimuthal separation, as indicated in the table. In addition to the 0.5-1.5 Hz passband, 0.5-1.0 Hz and 1.0-3.0 Hz passbands were also used. Among

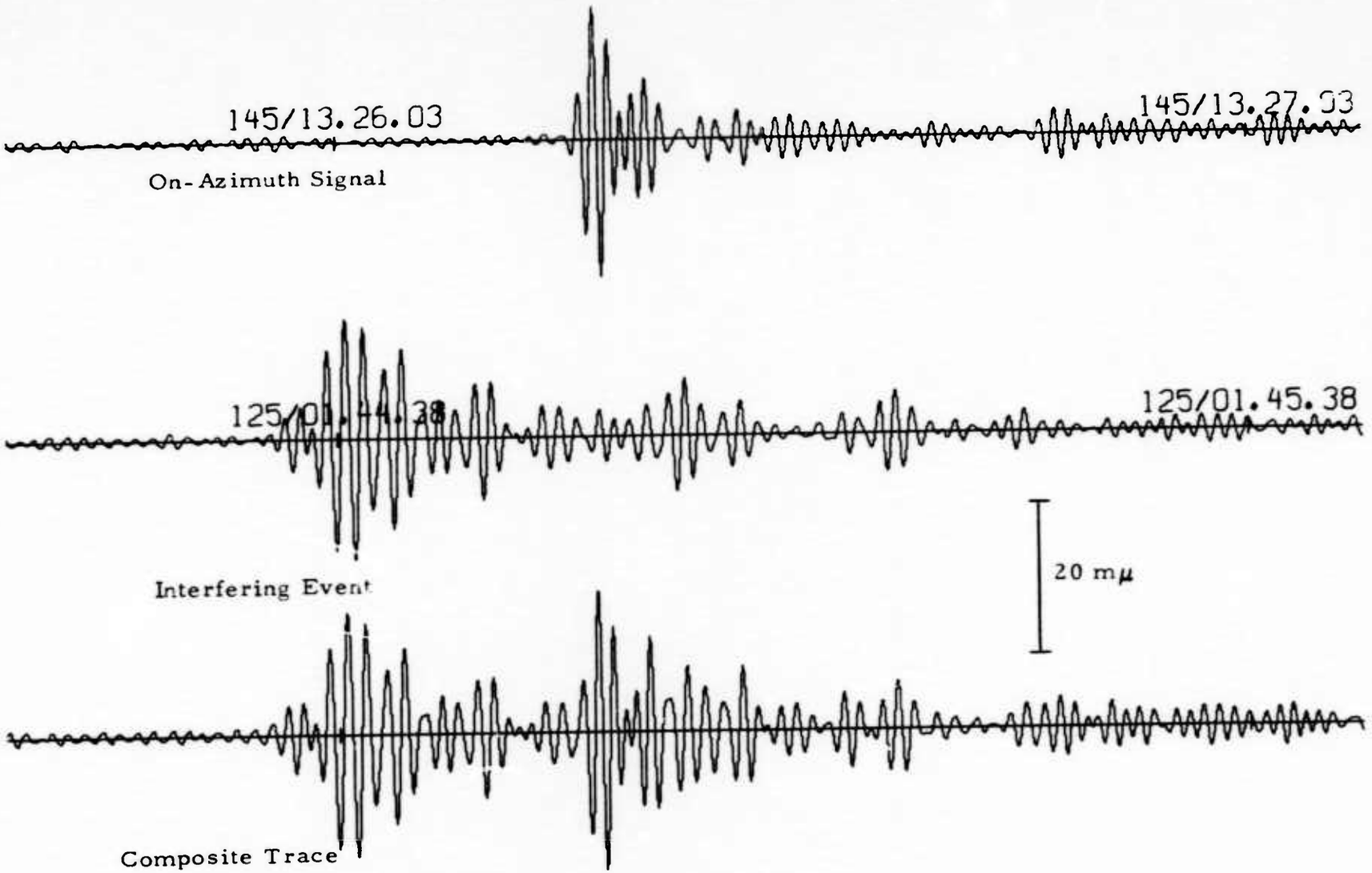

FIGURE II-15

BEAMSTEER OUTPUT FOR THE MIXED EVENT FROM DAYS 145 AND 125 OF 1973
(Signal Azimuth 47.6°, Signal Apparent Velocity 15.1 km/sec, Interfering Event Azimuth 227.6°, Interfering Event 3.1 dB Above the On-Azimuth Signal, 7 Sites and 0.5-1.5 Hz Passband)

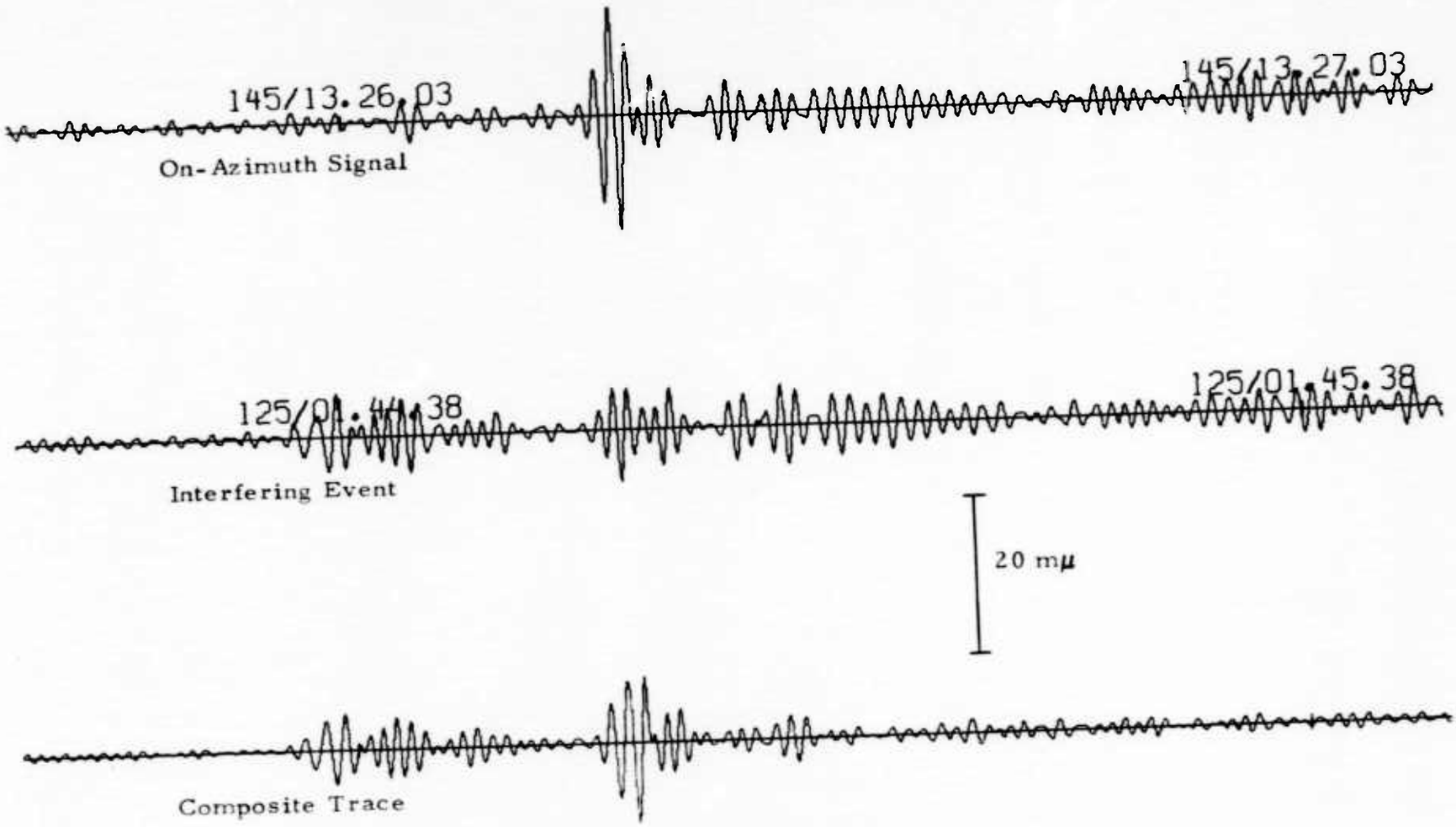

FIGURE II-16

ABF OUTPUT FOR THE MIXED EVENT FROM DAYS 145 AND 125 OF 1973
(μ = 0.5, Signal Azimuth 47.6°, Signal Apparent Velocity 15.1 km/sec, Interfering Event Azimuth 227.6°, Interfering Event 3.1 dB Above the On-Azimuth Signal, 7 Sites and 0.5-1.5 Hz Passband)

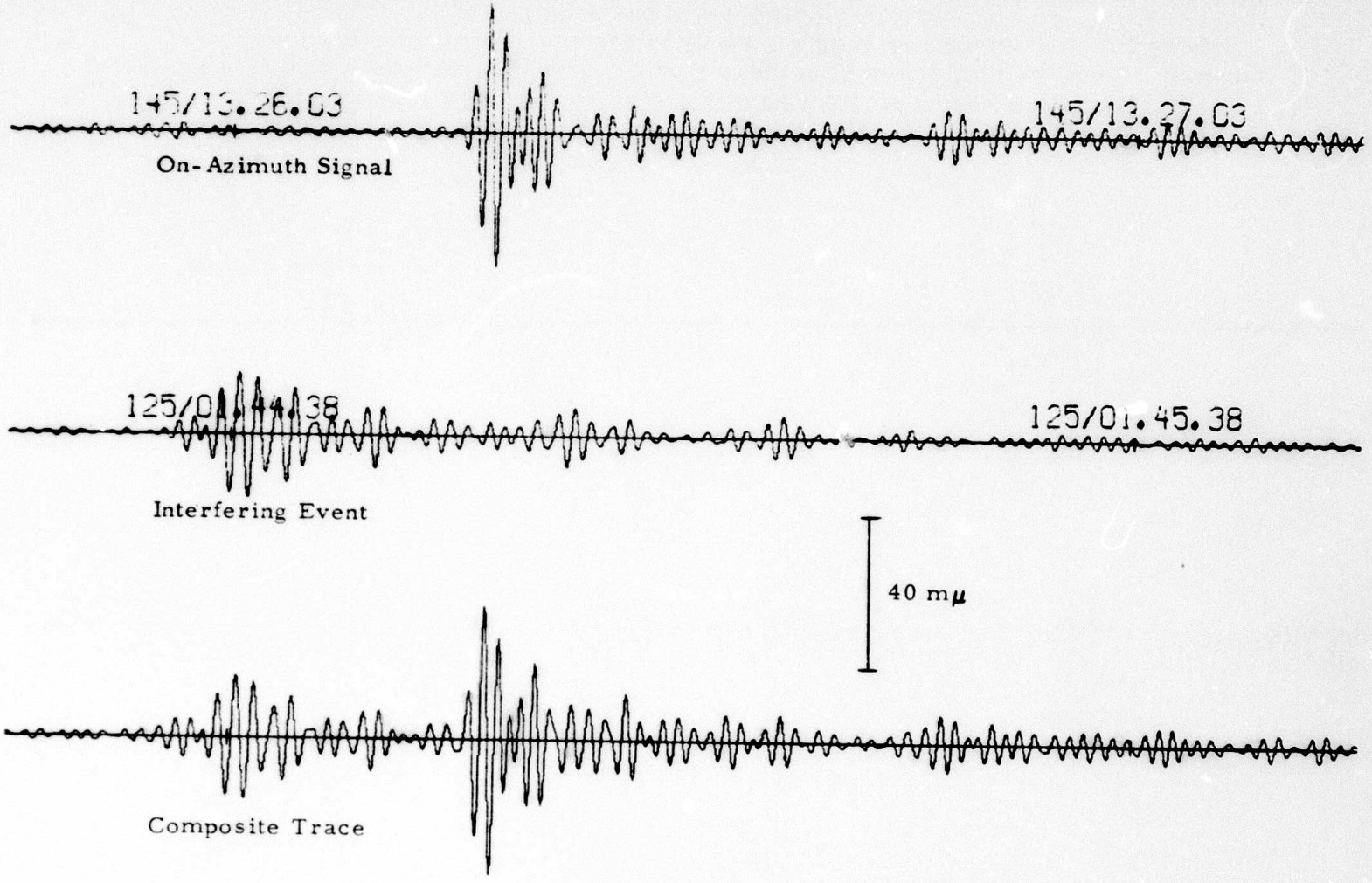

FIGURE II-17

BEAMSTEER OUTPUT FOR THE MIXED EVENT FROM DAYS 145 AND 125 OF 1973
(Signal Azimuth 47.6°, Signal Apparent Velocity 15.1 km/sec, Interfering Event Azimuth 227.6°, Interfering Event 2.4 dB Below the On-Azimuth Signal, 7 Sites and 0.5-1.5 Hz Passband)

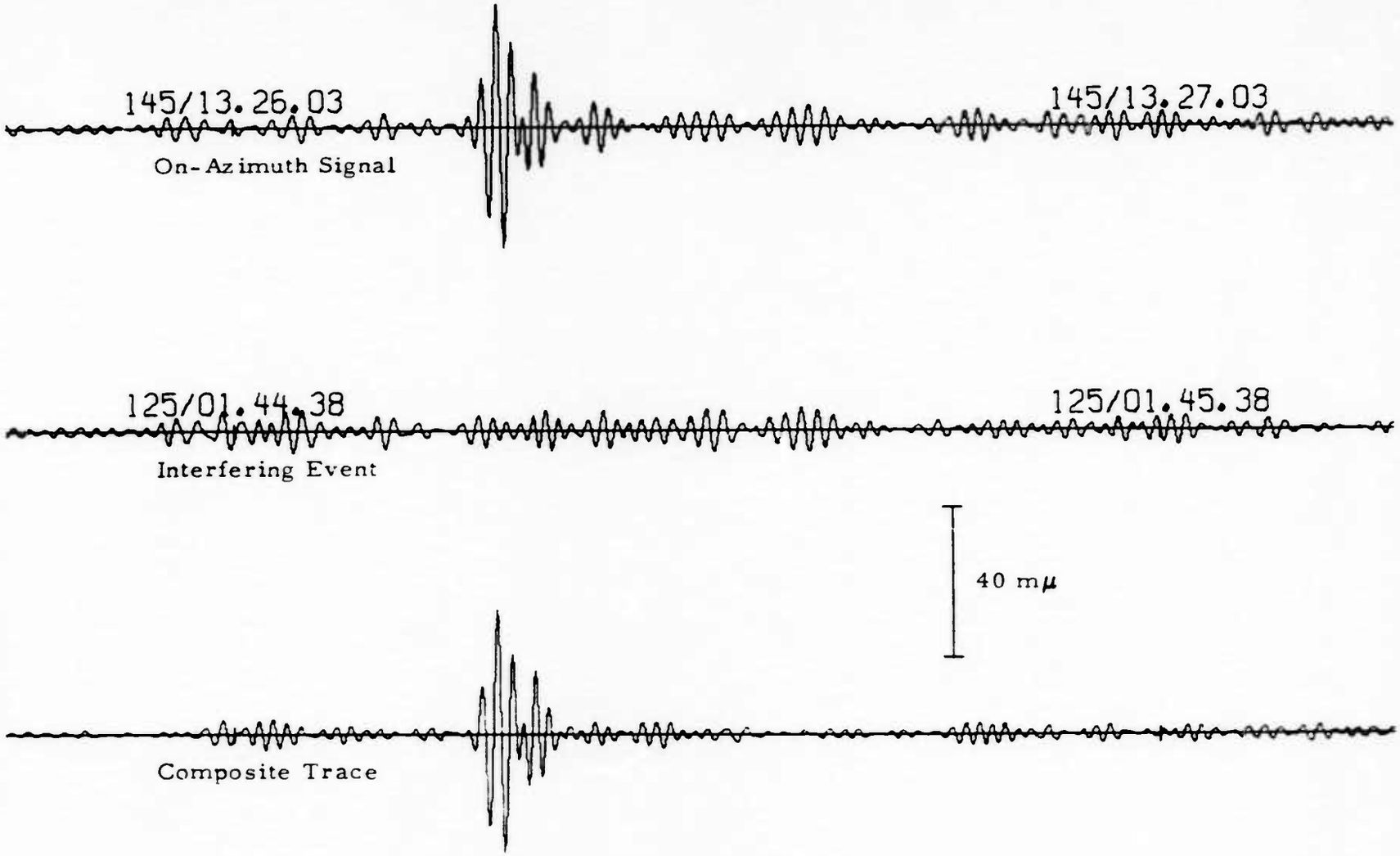

FIGURE II-18

ABF OUTPUT FOR THE MIXED EVENT FROM DAYS 145 AND 125 OF 1973
(μ = 0.5, Signal Azimuth 47.6°, Signal Apparent Velocity 15.1 km/sec , Interfering Event 2.4 dB Below the On-Azimuth Signal, 7 Sites and 0.5-1.5 Hz Passband)

TABLE II-5

AMPLITUDE RISE VALUES FOR VARIOUS CASES OF THE MIXED EVENT SIMULATION USING SEVEN-SITE INNER-RING ARRAY (ON-AZIMUTH EVENT FROM DAY 145, INTERFERING EVENT FROM DAY 125)

Pre-filter Pass-band (Hz)	ABF Filter Weights Per Channel (Points)	Azi-muthal Separa-tion	Best ABF Conver-gence Rate(μ)	Event Separa-tion(dB)	Beam-steer Ampli-tude Rise(dB)	Best ABF Ampli-tude Rise(dB)	ABF On-Azimuth Signal Attenuation Relative to Beam-steering(dB)	ABF Off-Azimuth Interfering Event Suppression Relative to Beam-steering(dB)	ABF Detec-tion Gain(dB)
0.5-1.5	11	180°	0.5	-18.8	-10.4	-3.9	7.2	13.7	6.5
0.5-1.5	11	90°	0.2	-18.8	-11.3	-1.6	4.1	13.8	9.7
0.5-1.5	31	180°	0.5	-18.8	-10.4	1.6	2.5	14.5	1.2
0.5-1.5	31	90°	0.5*	-15.3	-8.7	0.0	8.8	17.5	8.7
0.5-1.5	31	180°	0.5	-3.1	0.9	6.0	6.0	11.1	5.1
0.5-1.5	31	180°	0.5	2.4	-6.0	17.4	0.6	12.0	11.4
0.5-1.0	31	180°	0.4	-14.6	-10.6	-2.5	6.0	15.2	9.2
1.0-3.0	31	180°	0.1	-12.0	1.0	4.8	1.2	5.0	3.8

* Only one convergence rate was used

these passbands, the 0.5-1.5 Hz band produces the best results, as shown in Table II-5. In this simulation, adaptive beamforming achieved a substantial improvement relative to beamsteering. This improvement can be attributed mostly to the poor beamsteer performance at that steer velocity and passband. Figure II-19 shows the time-shift-and-sum beam pattern for the 47.6° steer azimuth and the 15.1 km/sec velocity at 1.0 Hz for the 7-site inner-ring array and the 19-site full array. The 7-site pattern is almost circular with unity response at the look direction and has a -6 dB value, in contrast to -20 dB for the 19-site pattern in the interfering-event separation. It reflects the low beamsteer array gain, which ranges from 3.6 dB to 8.4 dB for the 2.4 dB to -18.8 dB event separations, as shown in Table II-5.

This mixed-event simulation was repeated using the 19 sites of the full array as input channels. Figure II-20 shows the time-shift-and-sum beams for the 0.5 – 1.5 Hz passband. By increasing the number of sites to enlarge the aperture of array, a beamsteer array gain of nearly 20 dB was obtained. In contrast to the substantial ABF improvement relative to beamsteering achieved by using the 7-site array, acaptive beamforming using the 19-site full array provided no improvement with respect to the beamsteer results. Figure II-21 shows the best ABF beams at the convergence rate $\mu = 0.1$, where the amplitude rise on the composite trace is only comparable with the beamsteer output. However, one may be able to see a gap between the two event wavetrains on the adaptive composite-trace beam in Figure II-21. At the higher convergence rates, adaptive beamforming attentuates the on-azimuth signal rapidly so that the amplitude rise decreases. The adaptive beamformer, in order to minimize the power output, creates a waveform 180° out of phase with the upper trace on the interfering-event beam output and, as a result produces mutual cancellation on the composite trace. Figure II-22 illustrates these situations for the ABF beams at the convergence rate $\mu = 0.5$. In this mixed-event simulation, mutual cancellation appeared in other passbands at high convergence rates. Table II-6 tabulates the

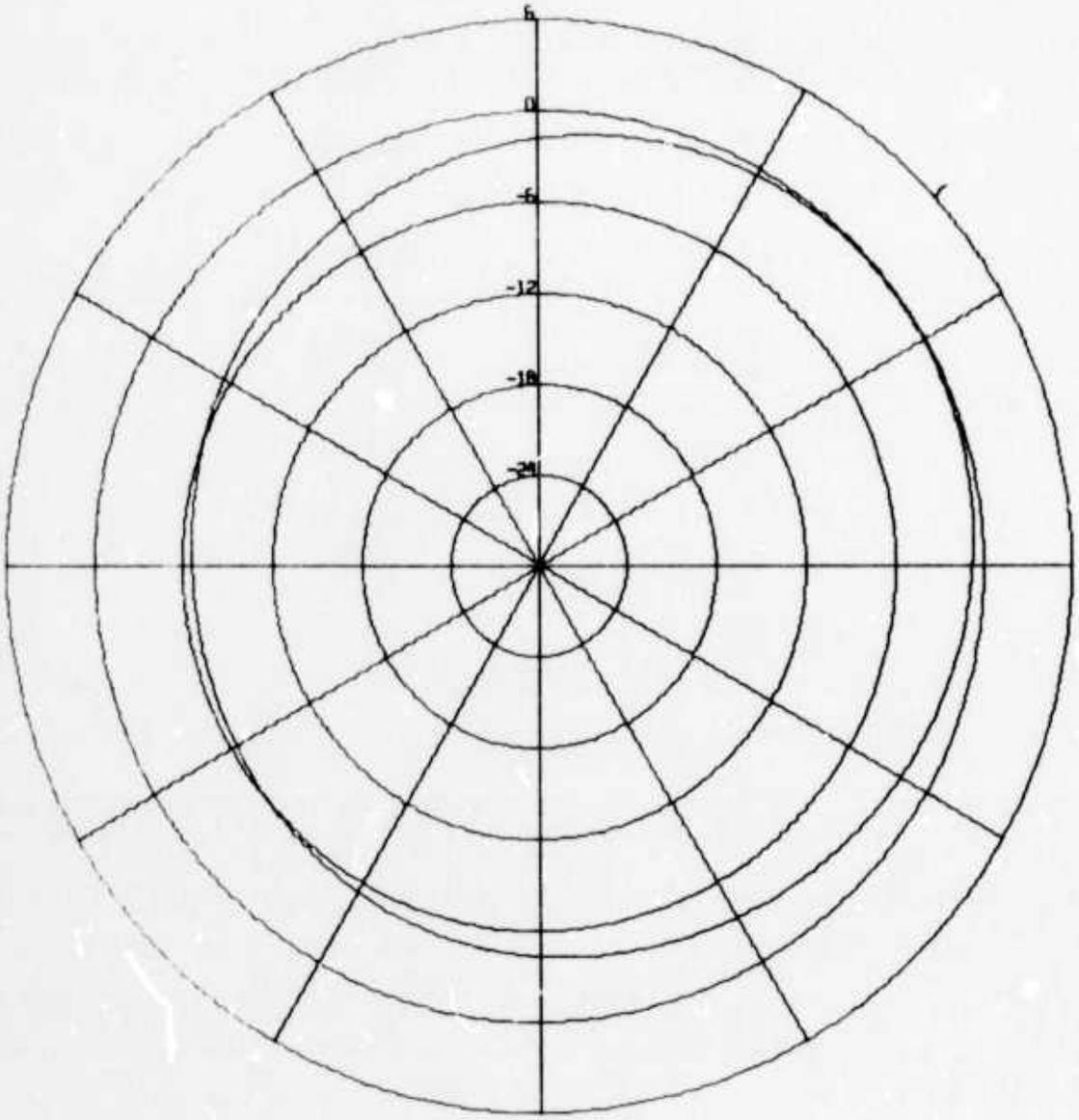

KOREA
TIME-SHIFT-AND-SUM BEAM PATTERN
BEAM LOOK VELOCITY IS 15.1, LOOK AZIMUTH 47.6
FREQUENCY IS 1.0 HZ. PERIOD 1.0 SECONDS

FIGURE II-19

INNER-RING AND FULL ARRAY BEAMSTEER RESPONSES
(7 Sites)
(PAGE 1 OF 2)

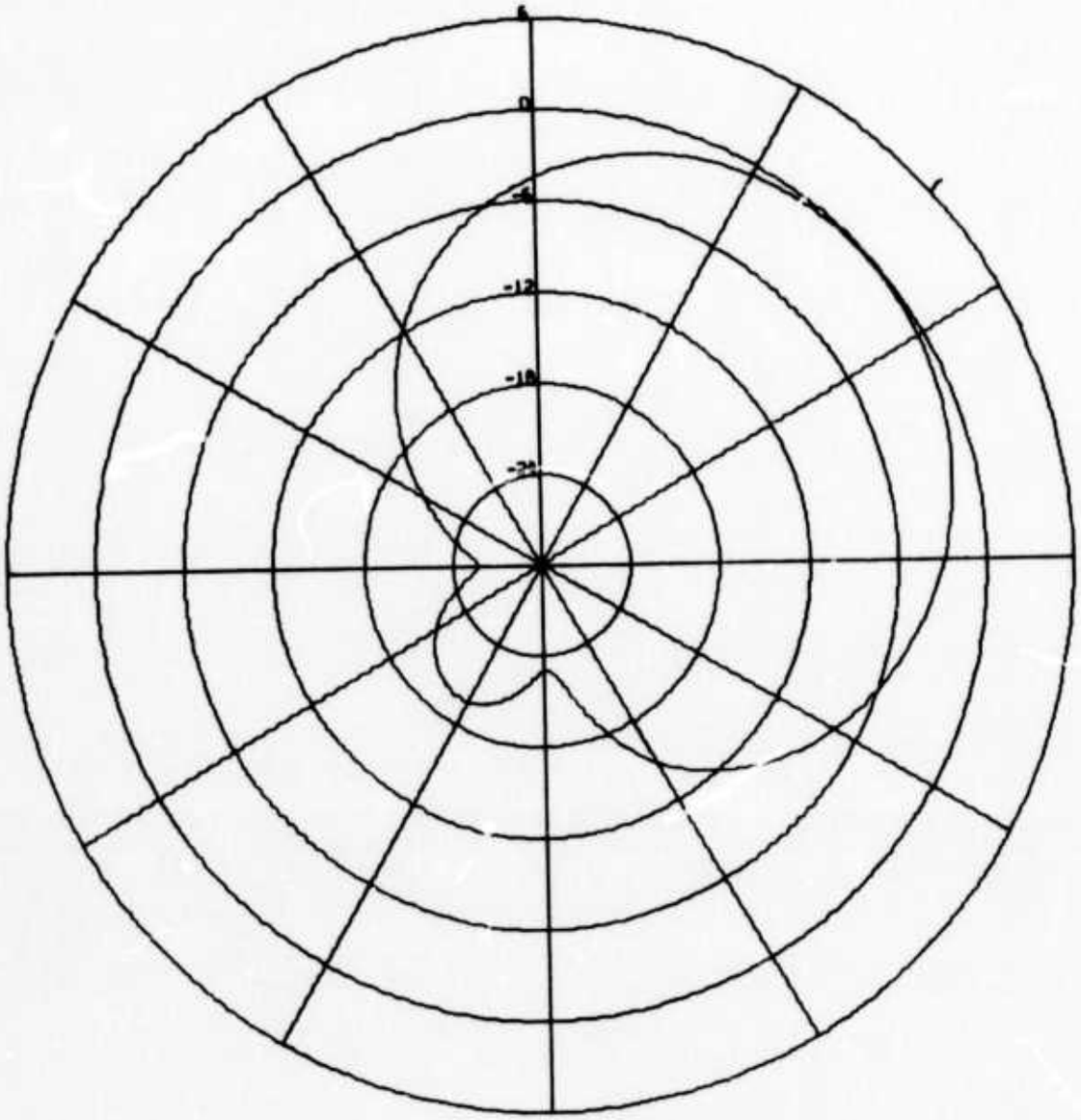

KOREA
TIME-SHIFT-AND-SUM BEAM PATTERN
BEAM LOOK VELOCITY IS 15.1, LOOK AZIMUTH 47.6
FREQUENCY IS 1.0 HZ, PERIOD 1.0 SECONDS

FIGURE II-19

INNER-RING AND FULL ARRAY BEAMSTEER RESPONSES
(19 Sites)
(PAGE 2 OF 2)

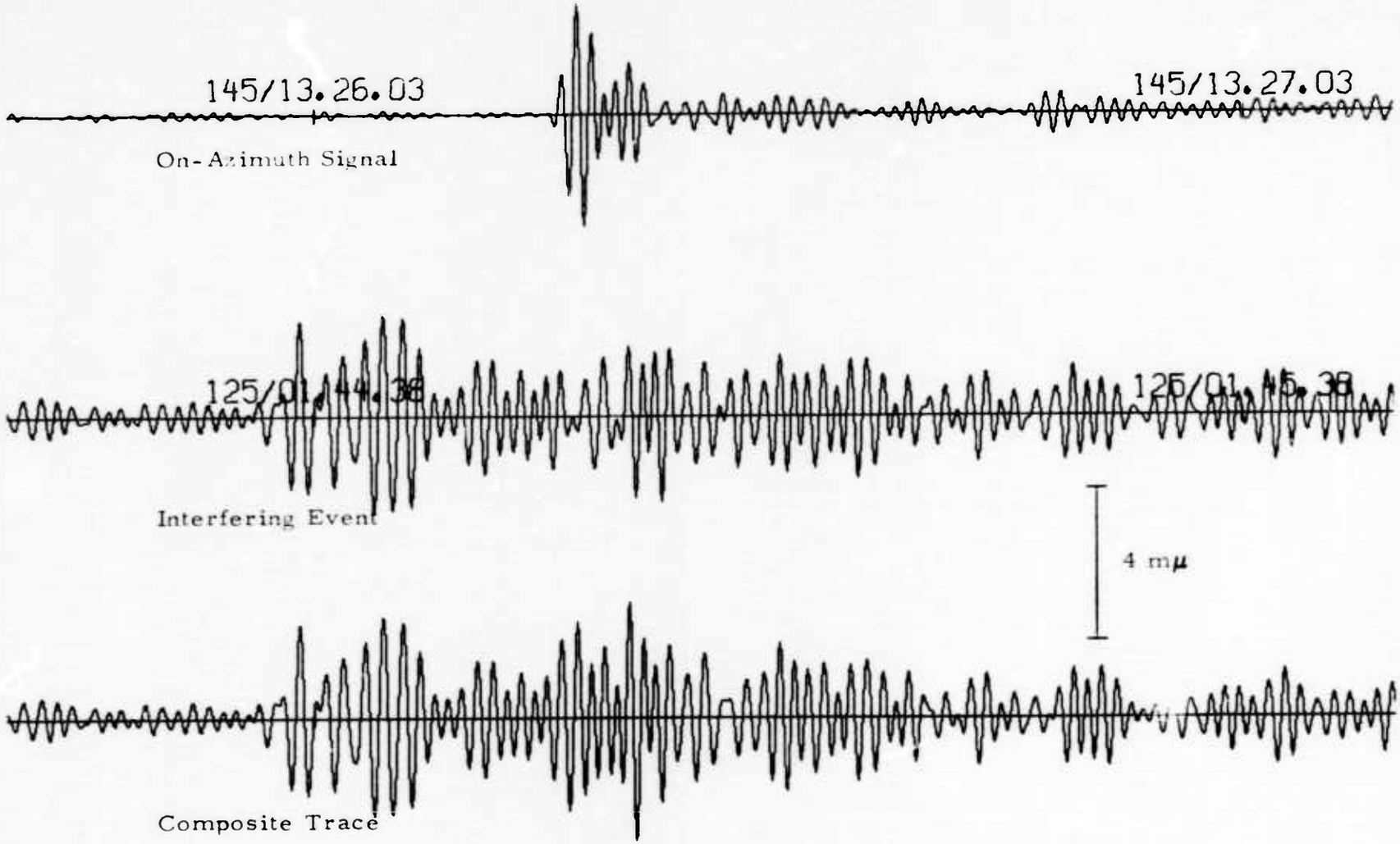

FIGURE II-20

BEAMSTEER OUTPUT FOR THE MIXED EVENT FROM DAYS 145 AND 125 OF 1973
(Signal Azimuth 47.6°, Signal Apparent Velocity 15.1 km/sec, Interfering Event Azimuth 227.6°, 18.8 dB Above the On-Azimuth Signal, 19 Sites and 0.5-1.5 Hz Passband)

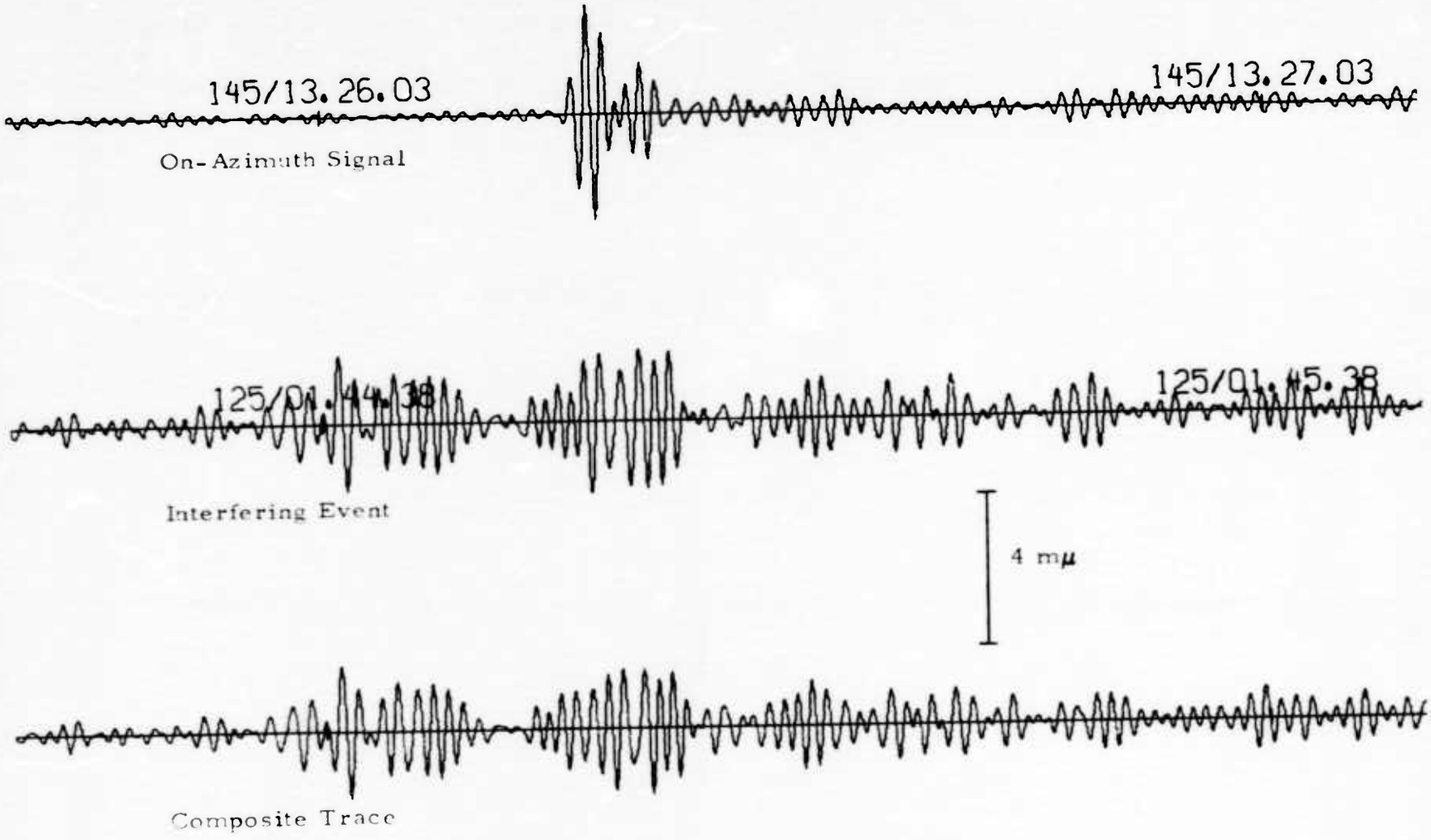

FIGURE II-21

ABF OUTPUT FOR THE MIXED EVENT FROM DAYS 145 AND 125 OF 1973 (Convergence Rate μ = 0.1, Signal Azimuth 47.6°, Signal Apparent Velocity 15.1 km/sec, Interfering Event Azimuth 227.6°, 18.8 dB Above the On-Azimuth Signal, 19 Sites, and 0.5-1.5 Hz Passband)

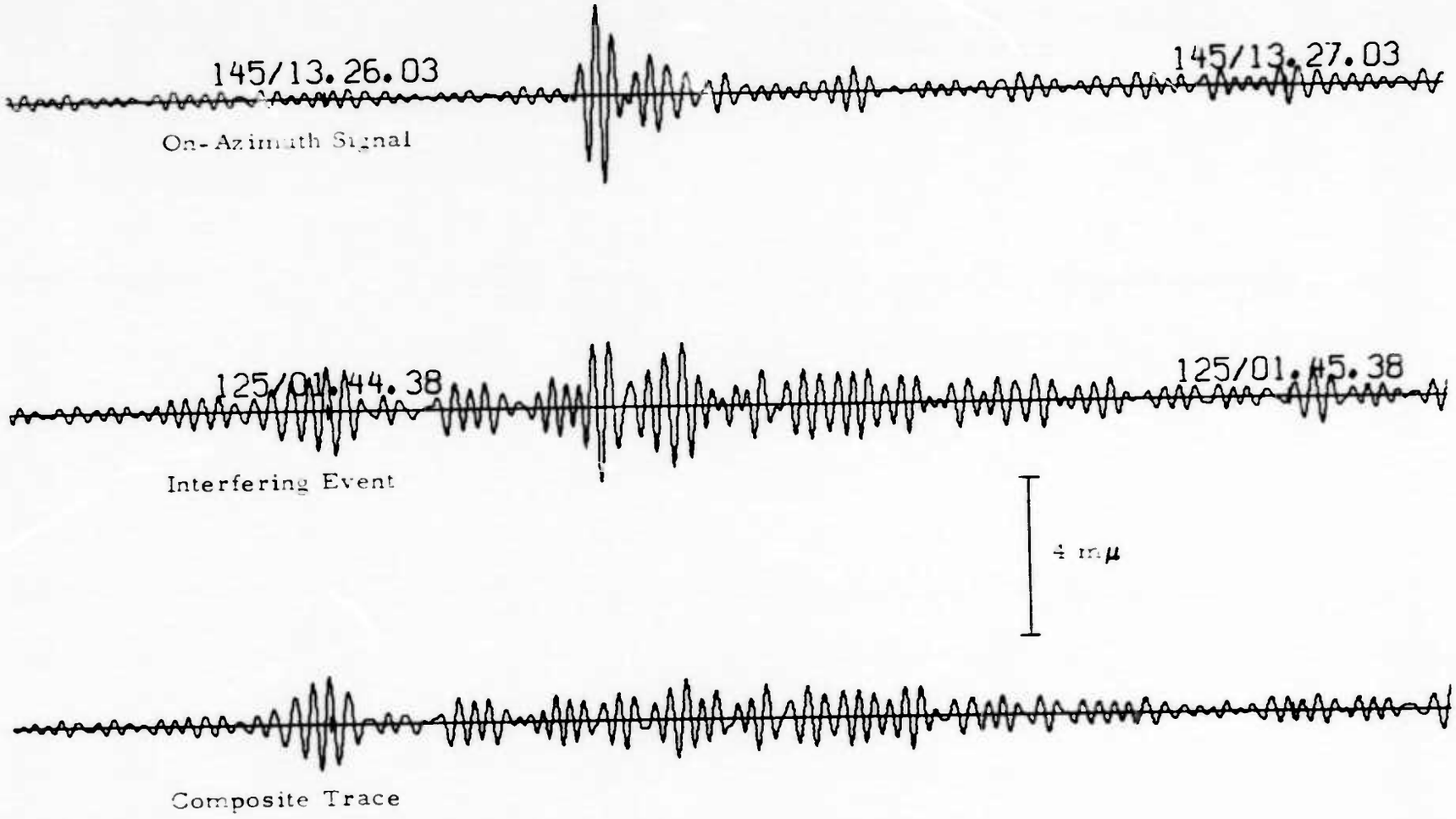

FIGURE II-22

ABF OUTPUT FOR THE MIXED EVENT FROM DAYS 145 AND 125 OF 1973
(μ = 0.5, Signal Azimuth 47.6°, Signal Apparent Velocity 15.1 km/sec, Interfering Event Azimuth 227.6°, Interfering Event 18.8 dB Above the On-Azimuth Signal 19 Sites and 0.5-1.5 Hz Passband)

TABLE II-6

AMPLITUDE RISE VALUES FOR VARIOUS CASES OF THE MIXED EVENT SIMULATION (ON-AZIMUTH EVENT FROM DAY 145, INTERFERING EVENT FROM DAY 125, 19 SITES)

Pre-filter Pass-band (Hz)	ABF Filter Weights Per Channel (Points)	Azi-muthal Separa-tion	Best ABF Conver-gence Rate(μ)	Event Separa-tion(dB)	Beam-steer Ampli-tude Rise(dB)	Best ABF Ampli-tude Rise(dB)	ABF On-Azimuth Signal Attenuation Relative to Beam-steering(dB)	ABF Off-Azimuth Interfering Event Suppression Relative to Beam-steering(dB)	ABF Detec-tion Gain(dB)
0.5-1.5	31	180°	0.1	-18.8	-0.4	-1.0	4.1	3.5	-0.6
0.5-1.5	11	180°	0.5	-18.8	-0.4	-3.5	14.0	10.8	-3.1
0.5-1.0	31	180°	0.1	-14.6	4.6	1.6	6.0	3.0	-3.0
1.0-3.0*	31	180°	0.1	-12.0	8.0	5.5	3.5	0.9	-2.5

* 17 Sites

amplitude-rise results for three passbands where only adaptive convergence rates greater than 0.1 were specified in the simulation.

6. Fourth Mixed-Event Simulation

The last mixed-event simulation was performed using the day 145 event from the south of Alaska as the on-azimuth signal and the day 169 event from off the coast of Hokkaido as the off-azimuth interfering event. Both the events have been used in the previous mixed-event simulations. In this mixed-event simulation, fourteen sites were used (all but sites 1, 2, 5, 9 and 15). The start times for the two events were adjusted so that the on-azimuth signal arrives 55 seconds after the arrival of the interfering event. In the previous simulations, where adaptive beamforming out performed beamsteering, the best adaptive processing results are usually at high convergence rates. However, in this simulation, mutual cancellation occurred at high convergence rates. As a result, the best adaptive processing results are only comparable to those of beamsteering. Table II-7 tabulates the amplitude rise results for the various processing parameters used. The 31-point adaptive filter length produces the best results among the three filter lengths specified for the 0.5-1.5 Hz passband. For the 1.0-2.0 Hz and 1.0-3.0 Hz passbands, the adaptive gains relative to beamsteering are only comparable to those of the 0.5-1.5 Hz passband, but both the adaptive and beamsteer array gains with respect to the single-sensor signal-to-noise ratio for these passbands are about 9.0 dB higher than those of the 0.5-1.5 Hz passbands, as shown in the table. For the 1.0-2.0 Hz and 1.0-3.0 Hz passbands, the beamsteer composite-trace amplitude increased, because of the interfering-event energy, by about 1.8 dB relative to the upper trace. This fact suggests that the low beamsteer array gain for the 0.5-1.5 Hz passband is due to the poor time-shift-and-sum beam pattern for that passband.

TABLE II-7

AMPLITUDE RISE VALUES FOR VARIOUS CASES OF THE MIXED EVENT SIMULATION (ON-AZIMUTH EVENT FROM DAY 145, INTERFERING EVENT FROM DAY 169, 14 SITES)

Pre-filter Pass-band (Hz)	ABF Filter Weights Per Channel (Points)	Azi-muthal Separa-tion	Best ABF Conver-gence Rate(μ)	Event Separa-tion(dB)	Beam-steer Ampli-tude Rise(dB)	Best ABF Ampli-tude Rise(dB)	ABF On-Azimuth Signal Attenuation Relative to Beam-steering(dB)	ABF Off-Azimuth Interfering Event Suppression Relative to Beam-steering(dB)	ABF Detec-t. Gain(dB)
0.5-1.5	15	180°	0.10	-12	-4.1	-4.9	6.0	5.2	-0.8
0.5-1.5	7	180°	0.20	-12	-4.1	-3.5	8.5	9.0	0.5
0.5-1.5	31	180°	0.10	-12	-4.1	-2.7	4.5	5.9	1.4
1.0-2.0	31	180°	0.05	-12	5.3	6.4	1.6	2.7	1.1
1.0-3.0	31	180°	0.05	-12	5.5	6.6	0.3	1.3	1.0

D. SUMMARY

In the first mixed-event simulation, the adaptive amplitude rise is about 2.0 dB higher than for beamsteering in most of the passbands processed except for the 0.5-1.5 Hz passband, in which the on-azimuth signal similarity is very poor. The adaptive processor can reduce the detection threshold 0.22 bodywave magnitude units on the basis of the mixed event single-sensor amplitude ratios at which a 6 dB amplitude rise occurs on the beamsteer and adaptive beam outputs. Adaptive beamforming is able to suppress the off-azimuth interfering event prior to the on-azimuth signal arrival, but it seems less effective in suppressing the off-azimuth event after the on-azimuth signal passes the array, particularly in the case of wider passbands.

The second mixed-event simulation employs the same on-azimuth signal as the first mixed-events and uses an off-azimuth interfering event with better signal similarity and a shorter duration than the first interfering event. The results are only slightly better than those of the first mixed-event simulation. However, for the cases where the interfering event was shifted to a 90^{o} azimuthal separation relative to the on-azimuth signal and where a 7-point adaptive filter length was used, a 0.55 m_b detection threshold reduction occurred with adaptive processing on the basis of the single-sensor signal-to-noise ratios at which a 6 dB amplitude rise occurred on the beamsteer and adaptive outputs.

In the third mixed-event simulation, the processing was performed using the 7-site inner-ring array and the 19-site full array. For the cases with the 7-site inner-ring array, the beamsteer array gain relative to a single sensor ranges from 3.6 dB to 8.4 dB, while the corresponding ABF array gain is from 12 dB to 20.4 dB. For the cases where beamsteering and adaptive beamforming achieve a 6 dB amplitude rise, adaptive beamforming reduces the detection threshold by 5.5 dB, or 0.28 m_b units. For the cases with the 19-site full array in the same mixed-event simulation, the best ABF amplitude rise is only close to, but not better than, that of the beamsteer output.

The last mixed-event simulation resulted in situations where mutual cancellation occurred on the adaptive beam outputs at high convergence rates and, as a result, the adaptive detection performance is only comparable to that of beamsteering. The average adaptive detection gain relative to beamsteering is about 0.6 dB for the five cases tried in this simulation.

In this mixed-event study, array processing gain is the difference between interfering-event suppression and signal degradation. For time-shift-and-sum beamforming, the processing gain is a constant for a given array configuration, steer velocity, passband, and look direction, and is independent of the event-separation level between the mixed events involved. However, in the case of signal degradation, the composite-trace signal amplitude was affected by addition or subtraction of interfering-event energy, which could produce inaccurate magnitude estimates. For example, in Table II-2, the composite-trace beamsteer signal amplitude is 3.4 dB higher than that on the upper trace. This higher value is due to the addition of the interfering event to the signal. For the optimum adaptive-beamforming processor in this case, both the upper trace and the composite trace have the same amplitudes, as shown in Table II-2, where their ratio is 0 dB at $\mu = 0.3$. As a consequence, the time-shift-and-sum beamformer registers a higher on-azimuth signal magnitude, and, in contrast, the adaptive beamformer provides an accurate measurement.

The results presented in this section are obtained from a maximum likelihood adaptive algorithm, where the design goal is to minimize the filter output power subject to unity-response constraints in the beam look direction. The adaptive performance here is not as good as its performance for long period ALPA data. Better detection might be possible with a Wiener time-domain adaptive algorithm, where the design goal is to minimize the mean square difference between the filter output and the on-azimuth signal.

SECTION III
CONCLUSIONS

In the mixed-event simulations presented in this report, two data samples, one with an on-azimuth signal and the other containing an interfering event, are summed to form a composite sample from which the adaptive filter sets are designed and applied to the two samples individually. The outputs of the two samples are added to form the composite beam used in simulating the actual situations encountered in practice. Amplitude-rise measurements are made by taking the ratio of the composite-trace maximum peak-to-peak amplitude after the signal arrival to the corresponding amplitude before the signal arrival.

The results vary from case to case. The following points summarize the results:

- In the first mixed-event simulation, where the interfering event has poor waveform similarity and time-varying relative amplitudes across the array, a 0.2 m_b detection threshold reduction with respect to the beamsteer level was obtained by adaptive beamforming. The second simulation uses the same on-azimuth signal as in the first and employs an off-azimuth interfering event with better waveform similarity. The results are slightly better than those of the first simulation. However, with a 7-point long adaptive filter and with a 90° azimuthal separation between the two events, adaptive beamforming was able to reduce the detection threshold by 0.5 m_b units from the beamsteer level.

Using the 7-site inner-ring array (sites 1 through 7), a detection threshold reduction of about 0.3 magnitude units relative to beamsteering was achieved in the third mixed-event simulation. In this case, the adaptive gain can be attributed to the poor time-shift-and-sum beam pattern. With the 19-site full array in this same simulation, the adaptive-processing results are only comparable to those of beamsteering because mutual cancellation occurs at high convergence rates. The last mixed-event simulation only produces comparable results between the adaptive and beamsteer processors due to the occurrence of mutual cancellation at high convergence rates.

- The beamsteer array gain relative to the single-sensor level is more affected by addition or subtraction of interfering-event energy than that of adaptive beamforming in this mixed-event study. As the event-separation level increases, the array gain tends to increase. For on-azimuth signal magnitude estimates, the adaptive-beamforming processor seems to produce more accurate results than beamsteering.

- Among the various passbands used, the 1-Hz-wide prefilter passband yielded the best results. The adaptive gain for various passbands is comparable as long as signal similarity does not vary significantly among the passbands. After the arrival of the on-azimuth signal, adaptive beamforming tends to suppress the off-azimuth interfering event less with the wider passbands.

- In these short-period P-wave mixed-event simulations, both the beamsteer and adaptive processors did not perform as well as in the long-period mixed-event simulation using ALPA data, particularly in the case of the adaptive processor. Signal similarity for the short-period P-wave signals from the spring 1973

Korea data is not as good as for the Rayleigh waves processed in the long-period study. Therefore, adaptive beamforming performs much better for the long-period Rayleigh waves than for the short-period P-waves.

In the spring of 1973, the Korean short-period arra data appeared to have some digitizer problems. Whether these problems have significant effects on the results presented in this report is still not known. The digitizer problems seem to be corrected in the November 1974 data. On the basis of a limited number of samples, the data quality during this period seems to have been greatly improved and seems to have better signal similarity across the array. Repeating this work with the November 1974 data might produce significantly better detection results.

SECTION IV
REFERENCES

Barnard, T. E., and L. J. O'Brien, 1974, An Evaluation of Adaptive-Beamforming Techniques Applied to Recorded Seismic Data, Technical Report No. 8, Texas Instruments Report Number ALEX(01)-TR-74-08, Contract Number F08606-74-C-0033, Texas Instruments Incorporated, Dallas, Texas.